

Supplemental Information for the following GEOLOGY submission

Don't judge an orogen by its cover: Kinematics of the Appalachian décollement from seismic anisotropy

Michael G. Frothingham¹, Vera Schulte-Pelkum^{1,2}, Kevin H. Mahan¹, Arthur J. Merschat³, Makayla Mather⁴, and Zulliet Cabrera Gomez⁴

¹Department of Geological Sciences, University of Colorado, Boulder, Colorado, 80309, USA

²Cooperative Institute for Research in Environmental Sciences, University of Colorado, Boulder, Colorado, 80309, USA

³U.S. Geological Survey, Florence Bascom Geoscience Center, Reston, Virginia, 20192, USA

⁴UNAVCO, Boulder, Colorado, 80301, USA

DESCRIPTION

This supplemental document includes captions for Tables S1-S3, Figures S1-S36, and captions for Figures S1-S36. Tables S1-S3 are attached separately as .xlsx files. Supplemental references cited are included at the end of this document.

Table S1. Structural attitudes (foliations, mylonitic foliations, and bedding) from the Greenville 1x2° quadrangle (Nelson et al, 1998). Attitudes were digitized using Geologic Map Data Extractor software (Allmendinger, 2020). The first row of column headers includes: latitude (deg, WGS84), longitude (deg), strike (deg, right-hand-rule), dip (deg, right-hand-rule), fabric type, the thrust sheet (from Nelson et al., 1998) that each attitude resides in, and the 7.5 minute USGS quadrangle that each attitude resides in. “TableS1.xlsx” is uploaded separately.

Table S2. Structural attitudes (lineations) from the Greenville 1x2° quadrangle (Nelson et al, 1998). Attitudes were digitized using Geologic Map Data Extractor software (Allmendinger, 2020). The first row of column headers includes: latitude (deg, WGS84), longitude (deg), trend (deg), plunge (deg), fabric type, the thrust sheet (from Nelson et al., 1998) that each attitude resides in, and the 7.5 minute usgs quadrangle that each attitude resides in. “TableS2.xlsx” is uploaded separately.

Table S3. Receiver function A1 arrivals from EarthScope SESAME and TA stations in the study area. Table includes the largest amplitude A1 arrival per station from conversions with: at least 50 traces, 0.6 to 5.94 s arrival times, A1 amplitude errors that are less than 60% of the A1 amplitude, and phase errors that are less than 20 degrees; following methods outlined in Schulte-Pelkum and Mahan (2014) and Frothingham et al. (2022). The first row of column headers includes: station name, station latitude (deg, WGS84), station longitude (deg), A1 arrival time (s), A1 amplitude (H/Z), bootstrap uncertainty maximum A1 amplitude, bootstrap uncertainty A1 minimum amplitude, A1 phase (= strike + 90, in deg), bootstrap uncertainty maximum phase, bootstrap uncertainty minimum phase, prominence, maximum azimuthal gap (deg), number of traces, and approximate A1 depth (km; = {A1 arrival time} x {8.47 km/s}). “TableS3.xlsx” is uploaded separately.

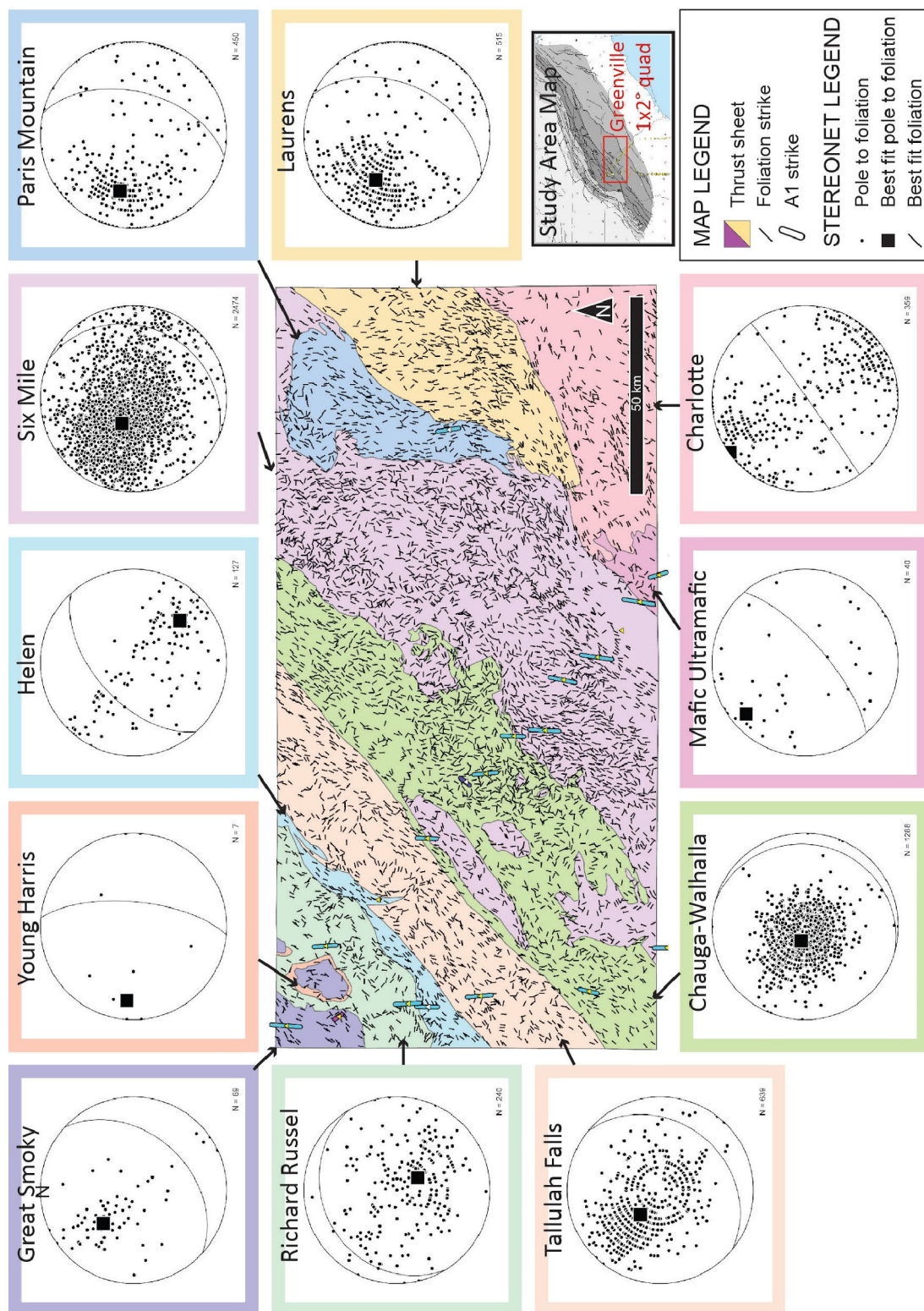


Figure S1. Structural analysis in the Greenville 1x2° quadrangle (Nelson et al, 1998). Map shows digitized foliations (black bars) and thrust sheets (colored polygons) from the Greenville 1x2° quadrangle (Nelson et al, 1998) as well as A1 arrival strikes (colored bars; from Fig. 1). Equal-area lower hemisphere stereonet plots digitized foliations and the best fit foliation per thrust sheet using Orient 3 software (Vollmer, 2015). Attitudes were digitized using Geologic Map Data Extractor software (Allmendinger, 2020).

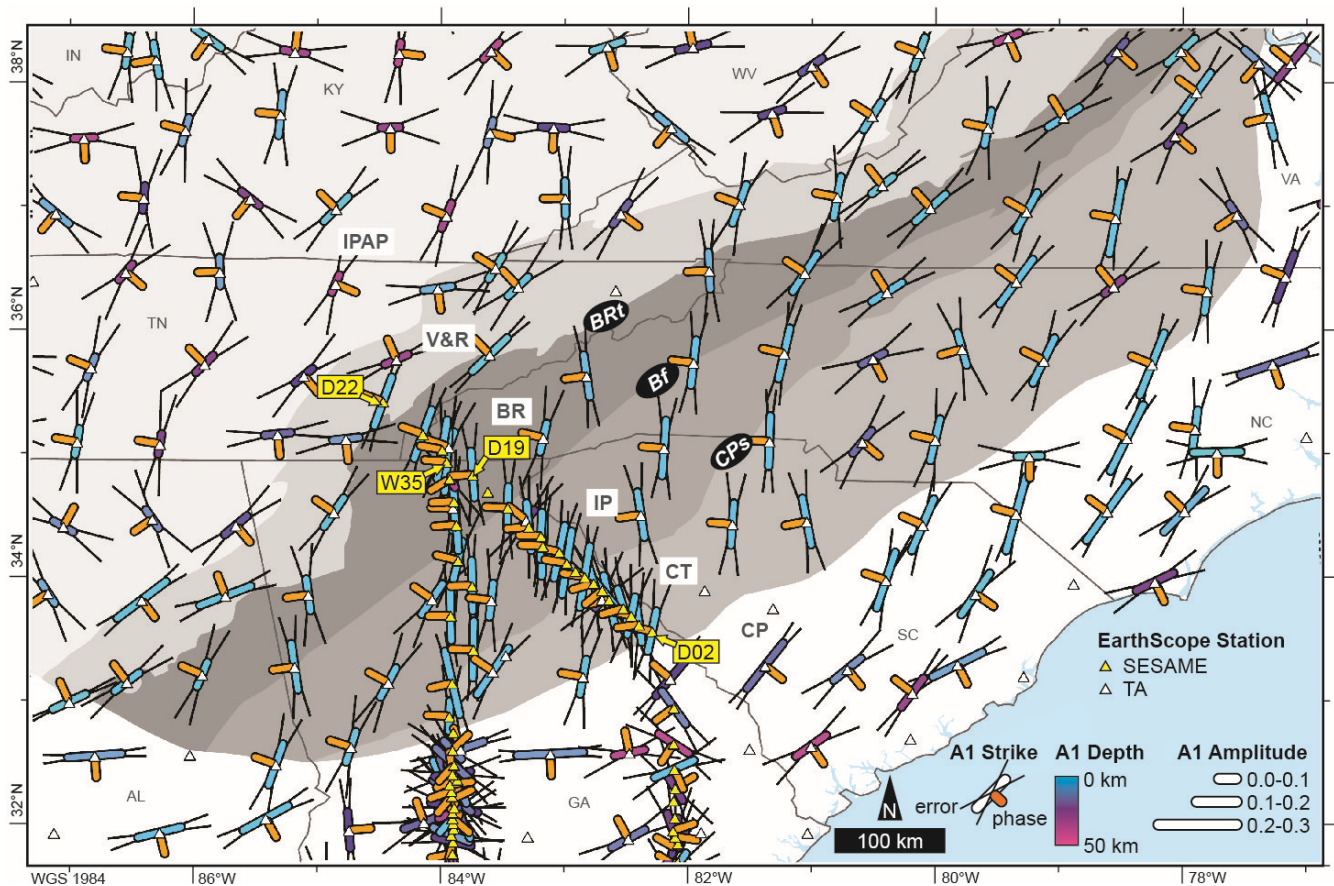


Figure S2. A1 phase and A1 strike errors. For each seismic station, the largest A1 arrival (blue to purple to pink bar) is oriented by strike, colored by depth, and sized by amplitude. Orange bar points towards A1 phase azimuth, which is the backazimuth of the peak positive polarity conversion (phase in Table S3). Phase (orange bar) does not necessarily point in the downdip or updip direction: such a distinction requires additional information (e.g., Schulte-Pelkum et al., 2020a). In our research, focusing on the southern BRP and the SESAME D-line, the orange phase bar generally points updip based on the assumption that the conversion occurs across a contrast (subhorizontal AD) between an overlying ~E dipping anisotropic foliation and underlying less anisotropic basement. Thin black lines are oriented in the maximum and minimum strike directions (perpendicular to p_{max} and p_{min} in Table S3), based on bootstrap error 95% confidence bounds. Tectonic provinces (Hatcher et al., 2007a) include Interior Plains-Appalachian Plateau (IPAP), Valley and Ridge (V&R), Blue Ridge (BR), Inner Piedmont (IP), Carolina Terrane (CT), and Coastal Plain (CP). BRP=BR+IP+CT. Faults include the Blue Ridge thrust (BRt), Brevard fault zone (Bf), and Central Piedmont suture (CPs). D22 to D02 mark cross section in Fig. 2. Figure is adapted from Fig. 1.

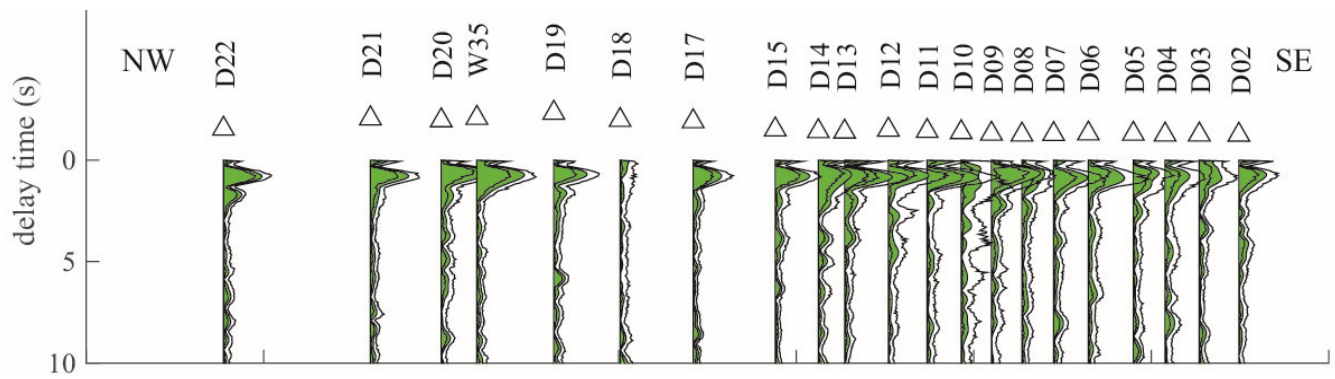


Figure S3. A1 trace profile for SESAME D-line and W35 stations, plotting A1 amplitudes (green) and bootstrap error 95% confidence bounds (black). AD has prominent arrivals near 1 s. Refer to Fig. 1 for profile location. Modified from Fig. 2b.

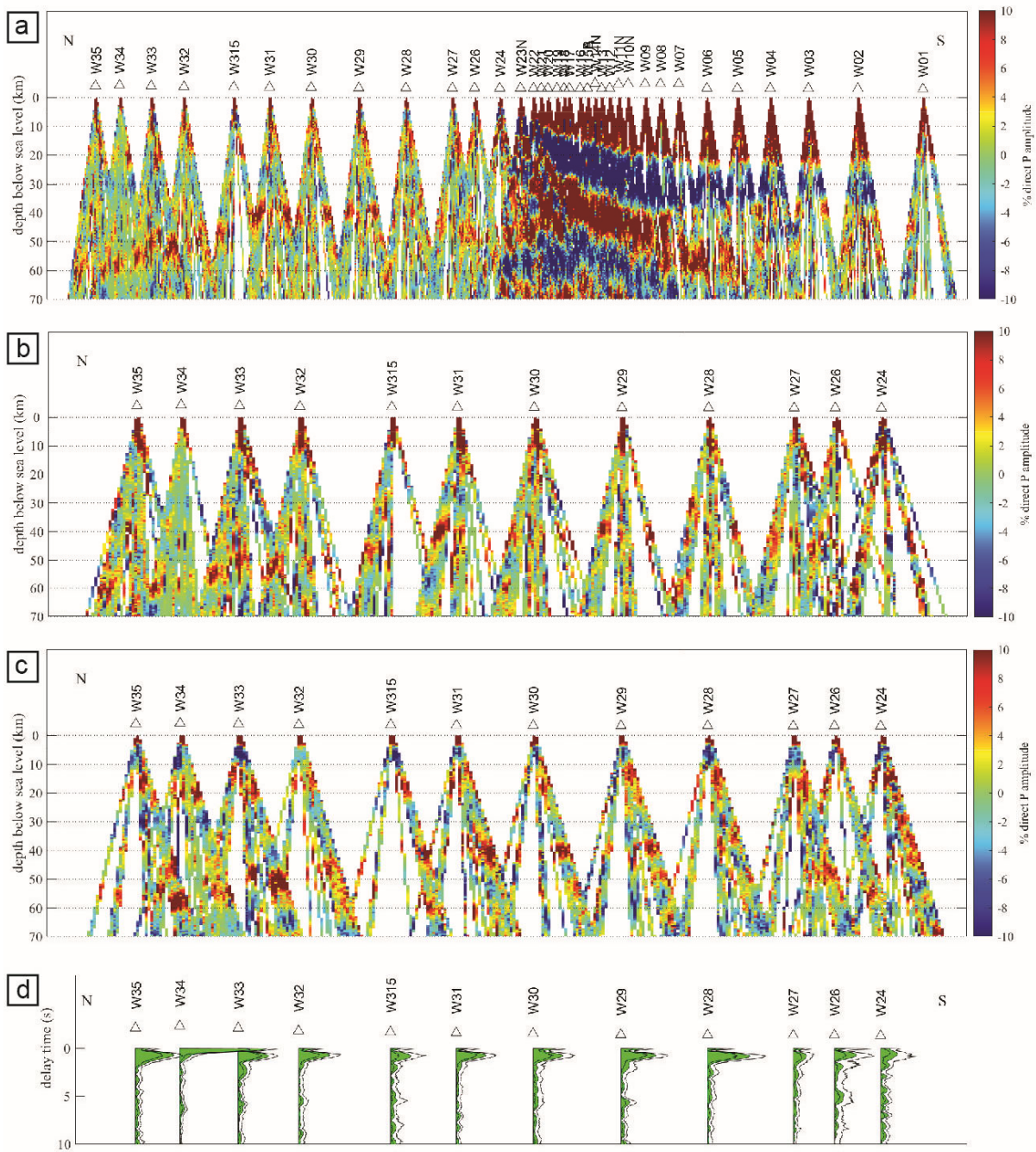


Figure. S4. (a) Radial component unsmoothed common conversion point (CCP) stack for SESAME W-line stations, including stations from the coastal plain. Refer to Fig. 1 for profile location. Plot shows conversions from all azimuths. Stations in the coastal plain (W23N to W01) show sediment reverberations that are absent at stations in the Valley and Ridge and Blue Ridge-Piedmont. (b) Radial component unsmoothed CCP stack for SESAME W-line stations (excluding stations from the coastal plain). Plot shows raypaths from western backazimuths only (excludes eastern backazimuths). (c) Same as (b), but shows raypaths from eastern backazimuths only (excludes western backazimuths). AD has prominent arrivals between 5-10 km in: (b) with positive (red) polarity from western backazimuths and (c) with negative (blue) polarity from eastern backazimuths. (d) A1 trace profile for SESAME W-line stations (excluding stations from the coastal plain) plots A1 amplitudes (green) and bootstrap error 95% confidence bounds (black). Adapted from Fig. 2.

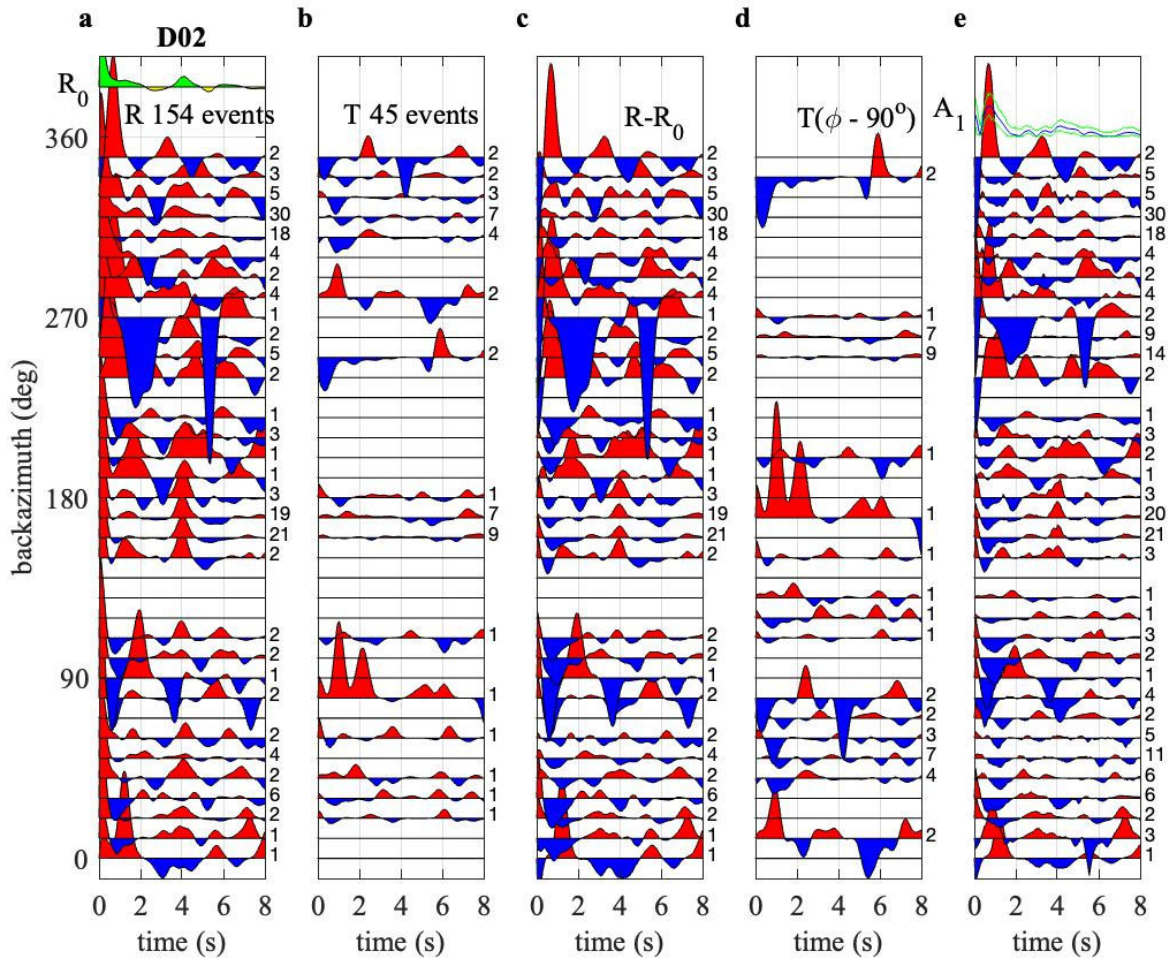


Figure S5. SESAME station D02 receiver functions and first harmonic solutions. (a) Radial component receiver function, corrected for slowness and binned by backazimuth (number of events per bin on the right). Each receiver function is corrected to vertical incidence in time and to a common incidence angle in amplitude before binning. R_0 (green and yellow) is average over azimuthal bins. (b) As in (b), but transverse component. (c) Radial component receiver functions after subtracting R_0 . (d) Transverse component receiver functions shifted in backazimuth by 90° to match $R-R_0$. (e) Traces in (c) and (d) binned together; this is the input for the azimuthal harmonic decomposition. First harmonic solution amplitude (A_1 , blue line) with bootstrap error 95% confidence bounds (green lines) from a moving window harmonic decomposition of the signal in (e) calculated as in Schulte-Pelkum and Mahan (2014). Additional information for the largest A_1 arrival is in Table S3. A worked example for station D02, from data in Table S3, is as follows. Largest A_1 arrival occurs at 0.71 s (6.01 km), see blue line amplitude peak in the top of (e). Phase (positive polarity amplitude arrival) is -78.1° (281.9° backazimuth in panel e). Strike (undirected $\pm 180^\circ$) is 11.9° and 191.9° backazimuth (Phase $\pm 90^\circ$). Strike is approximately located at polarity flips (red to blue) in panel (e). Other station examples can be worked via subsequent figures and accompanying data in Table S3.

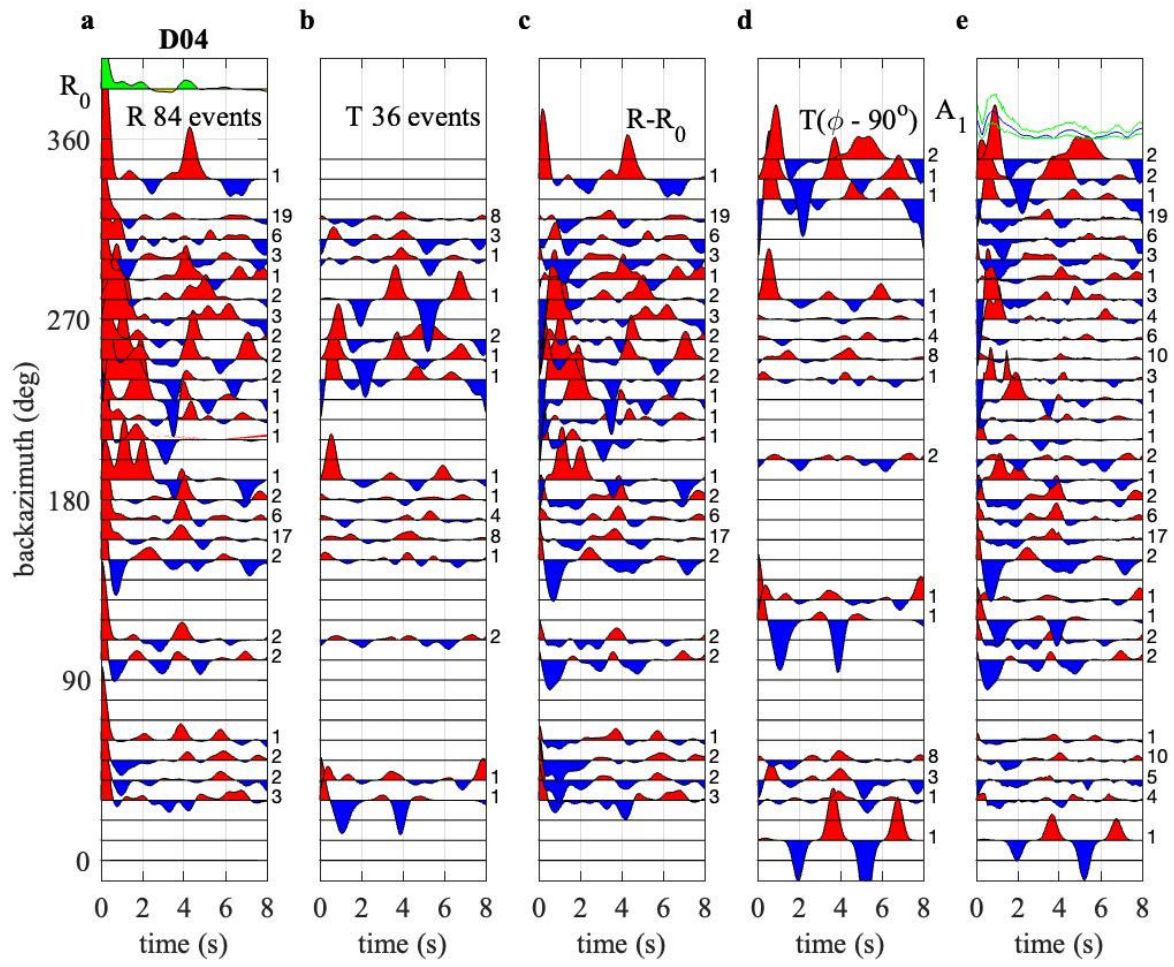


Figure S7. As in Fig. S5, but for SESAME station D04.

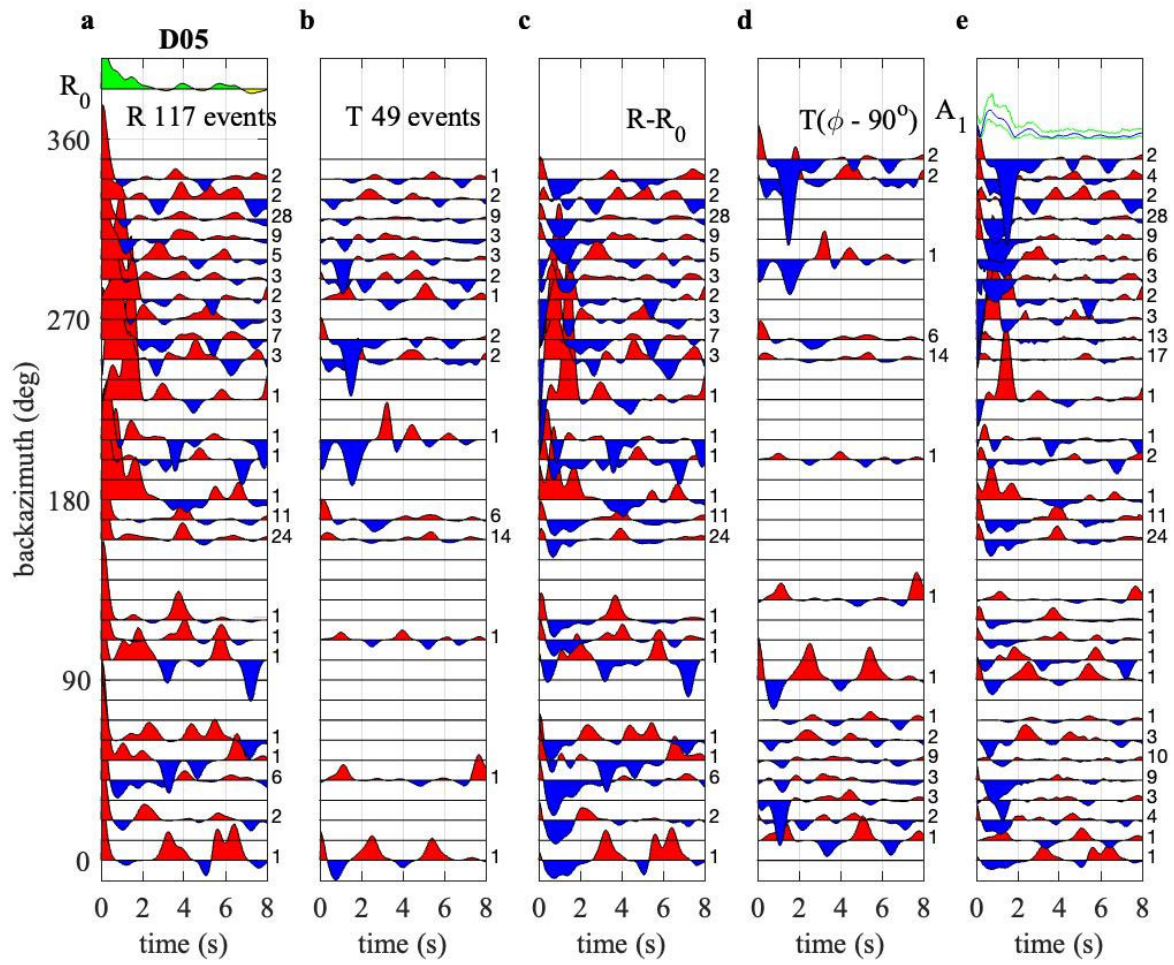


Figure S8. As in Fig. S5, but for SESAME station D05.

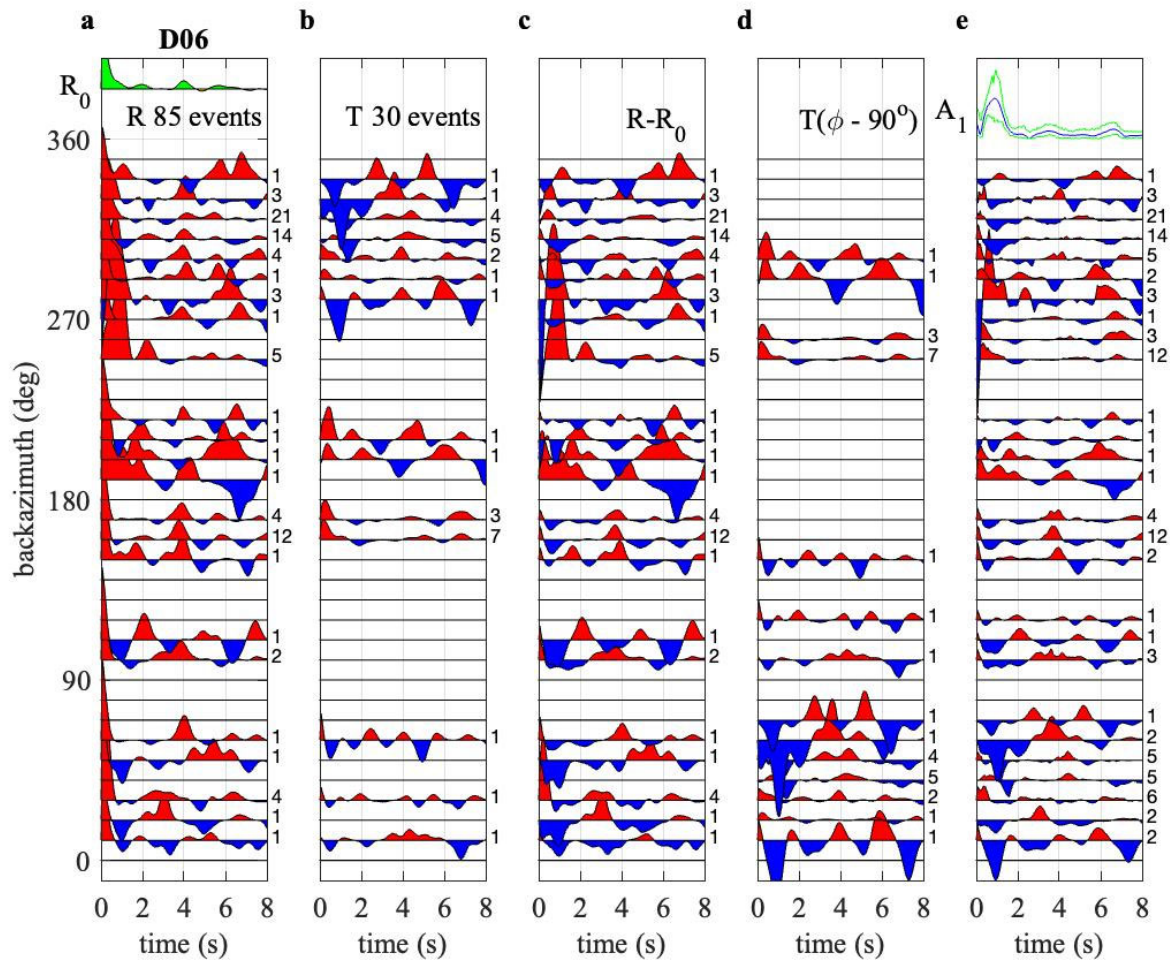


Figure S9. As in Fig. S5, but for SESAME station D06

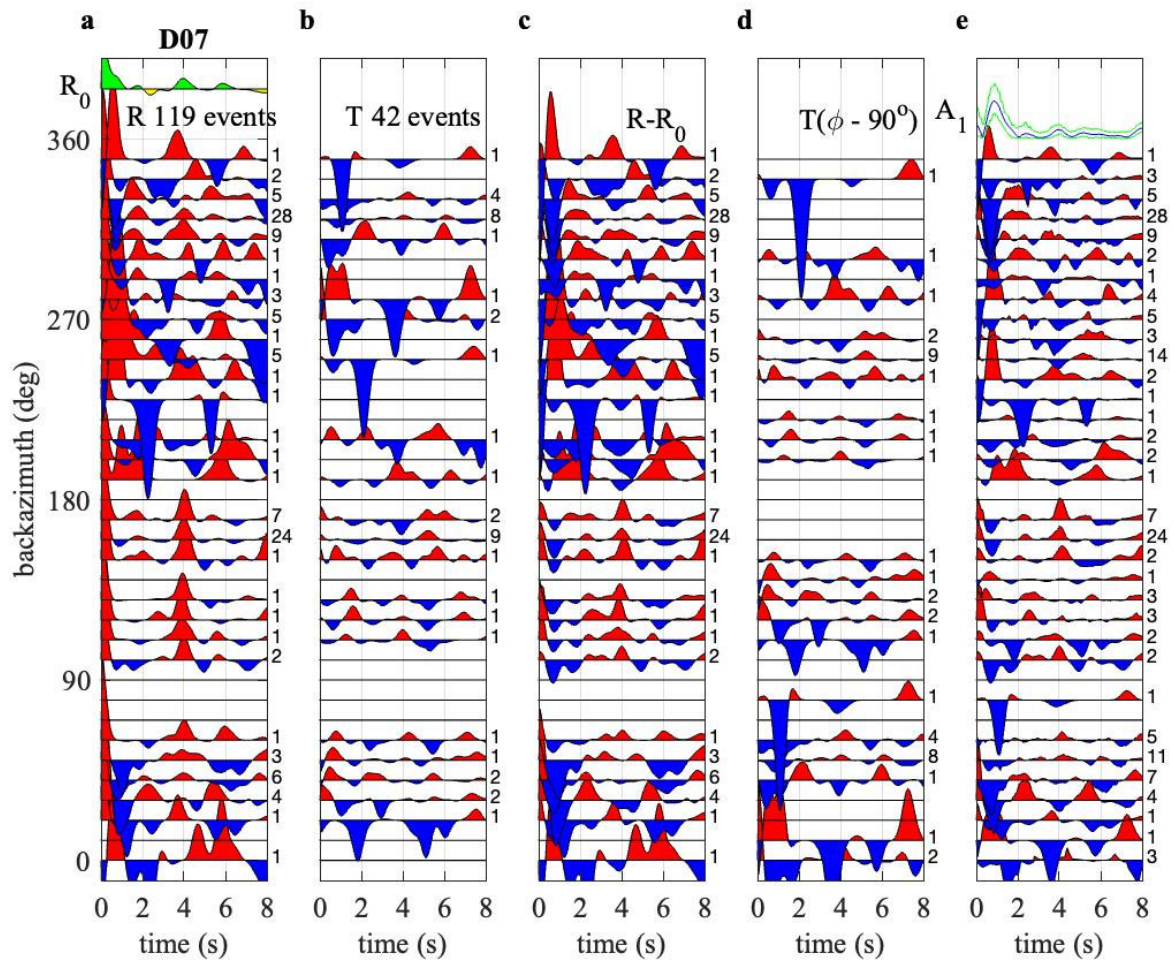


Figure S10. As in Fig. S5, but for SESAME station D07.

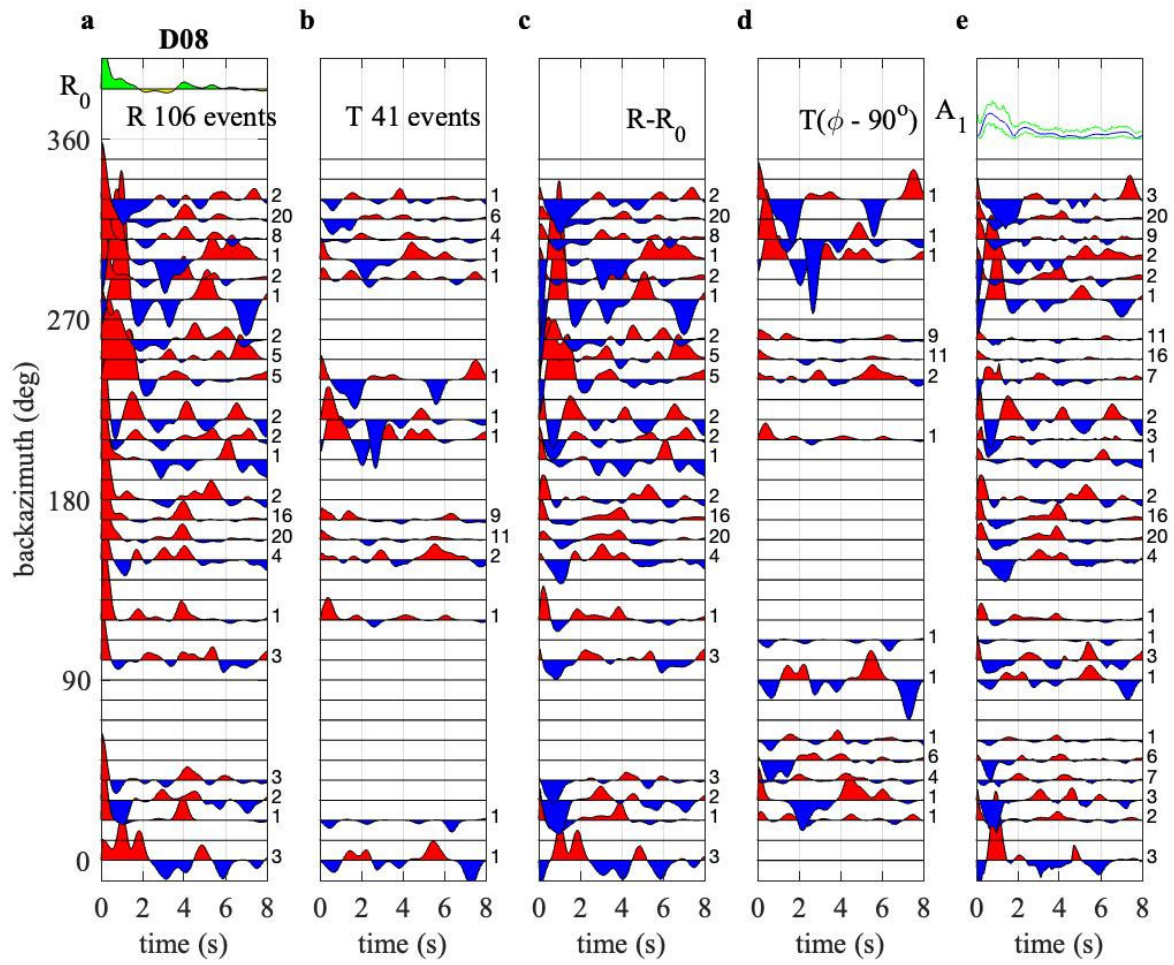


Figure S11. As in Fig. S5, but for SESAME station D08.

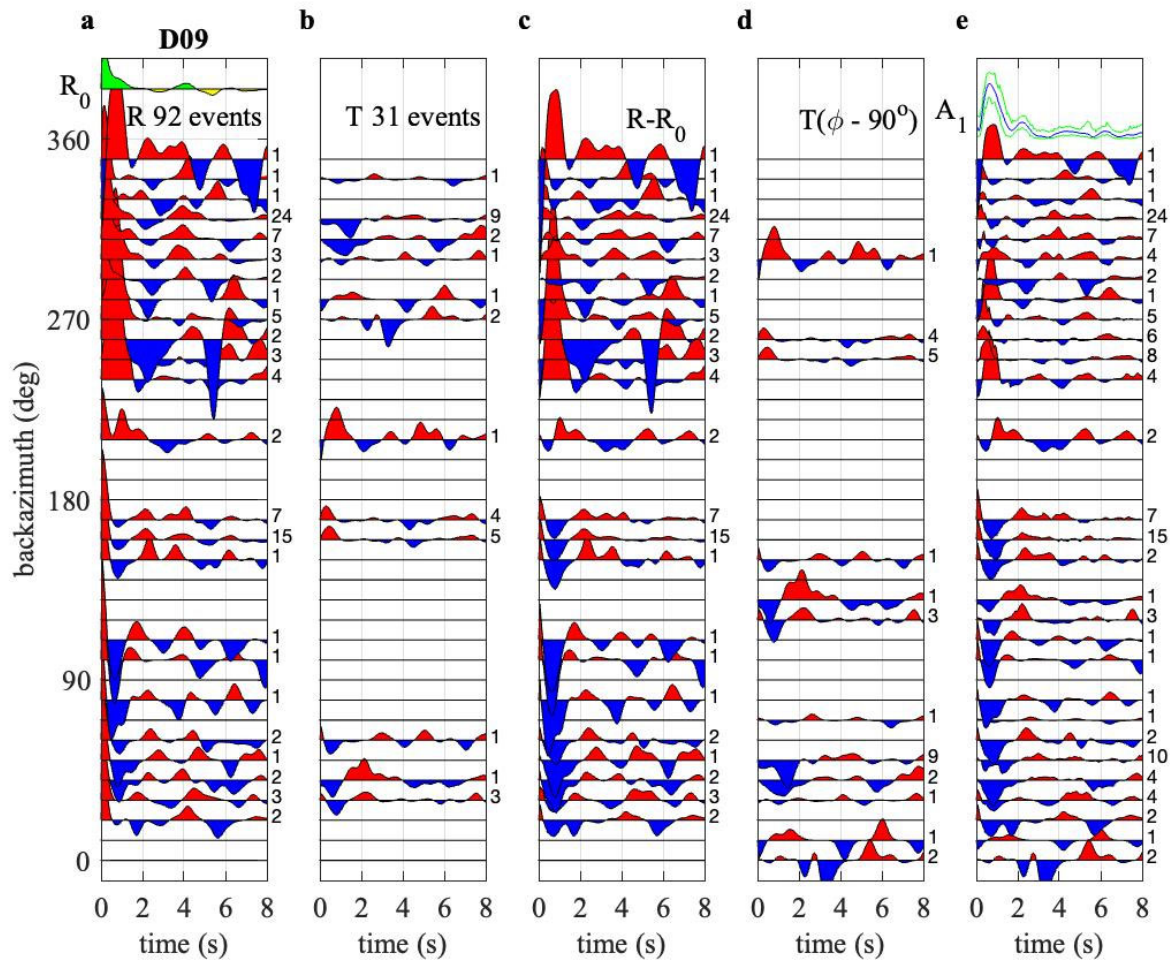


Figure S12. As in Fig. S5, but for SESAME station D09.

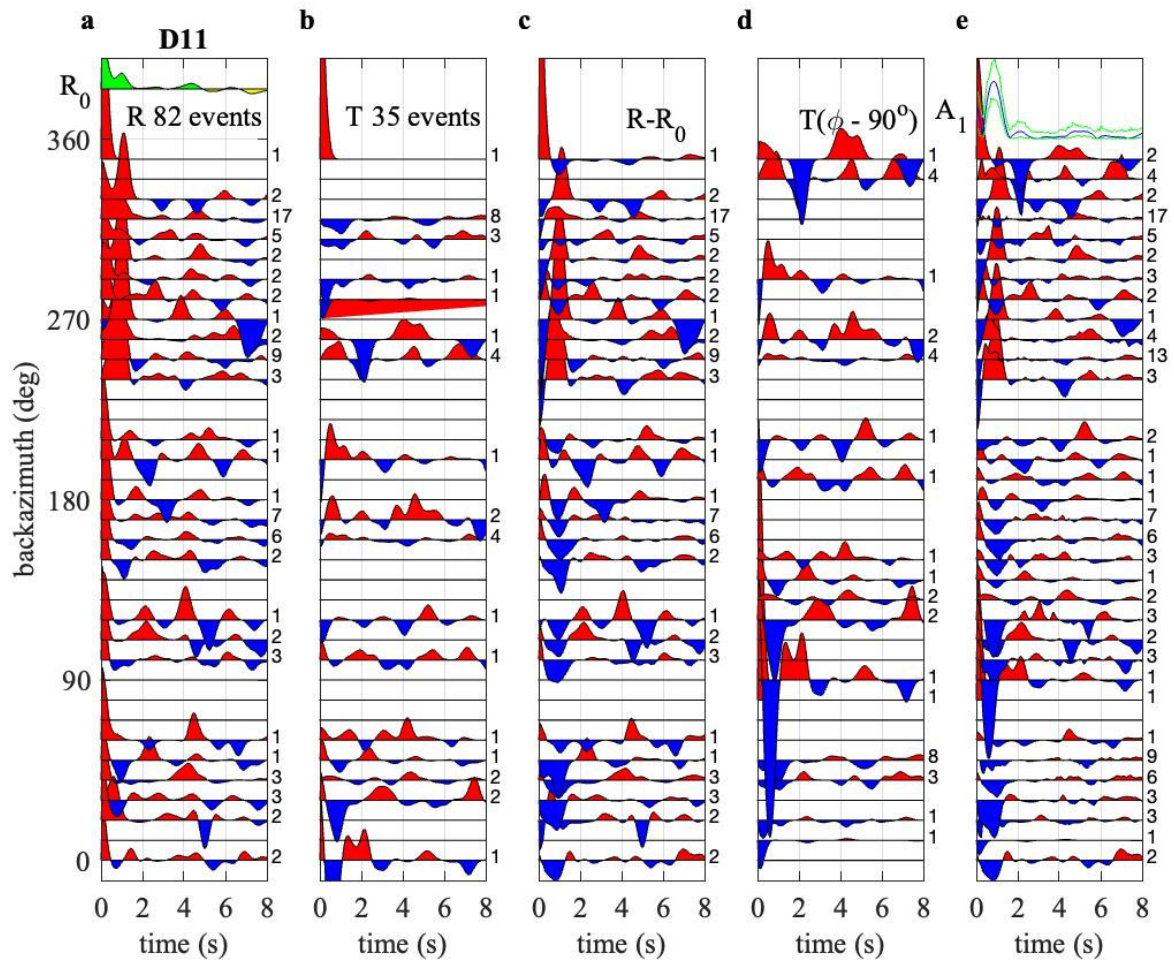


Figure S14. As in Fig. S5, but for SESAME station D11.

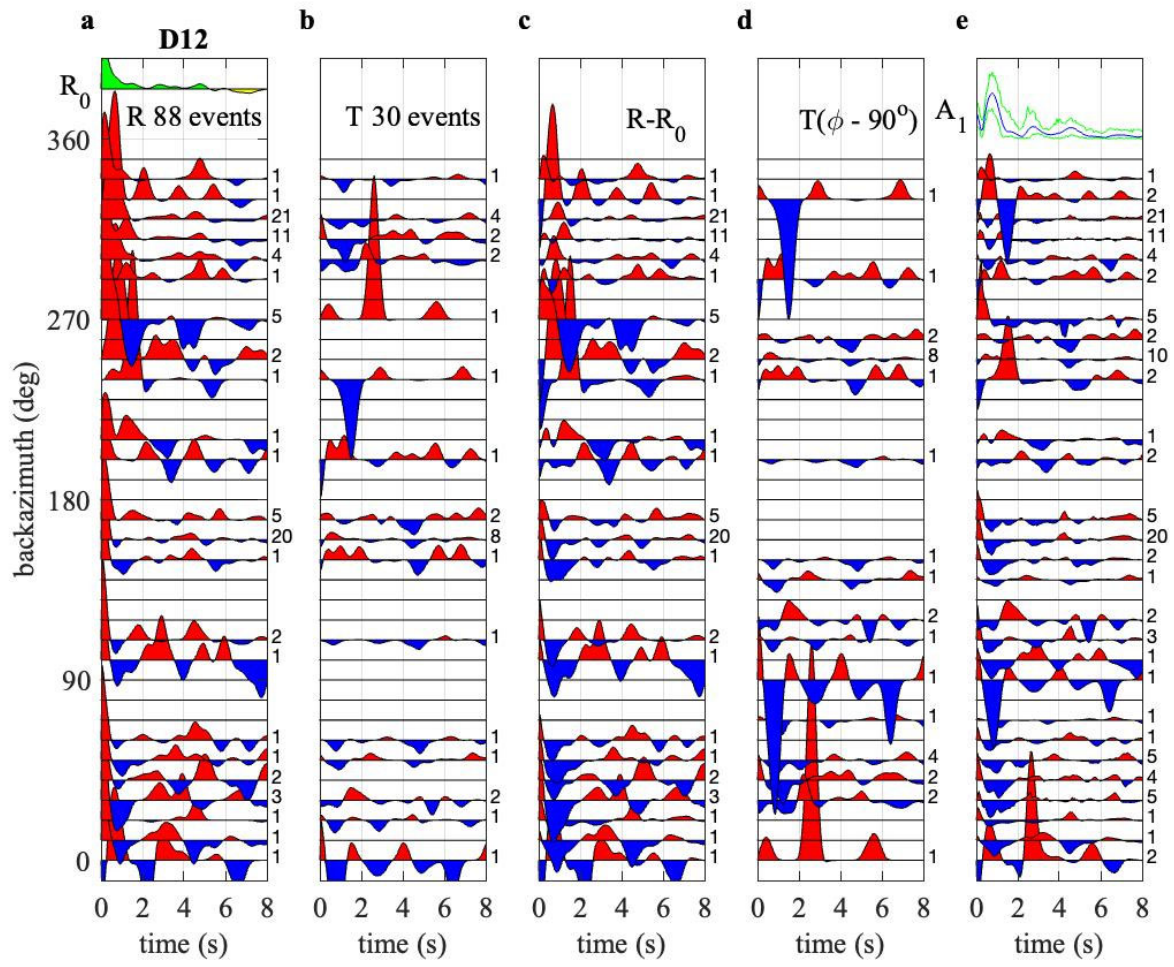


Figure S15. As in Fig. S5, but for SESAME station D12.

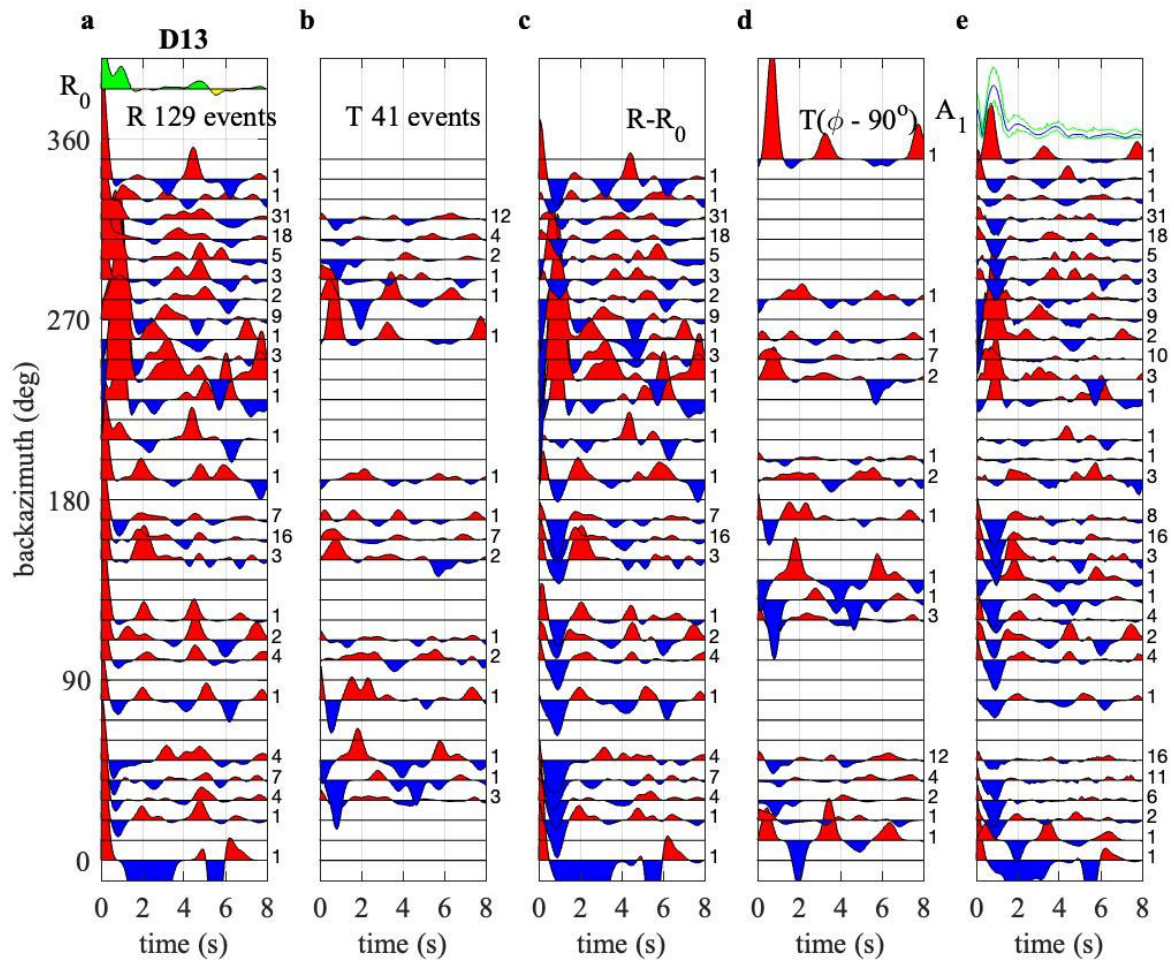


Figure S16. As in Fig. S5, but for SESAME station D13.

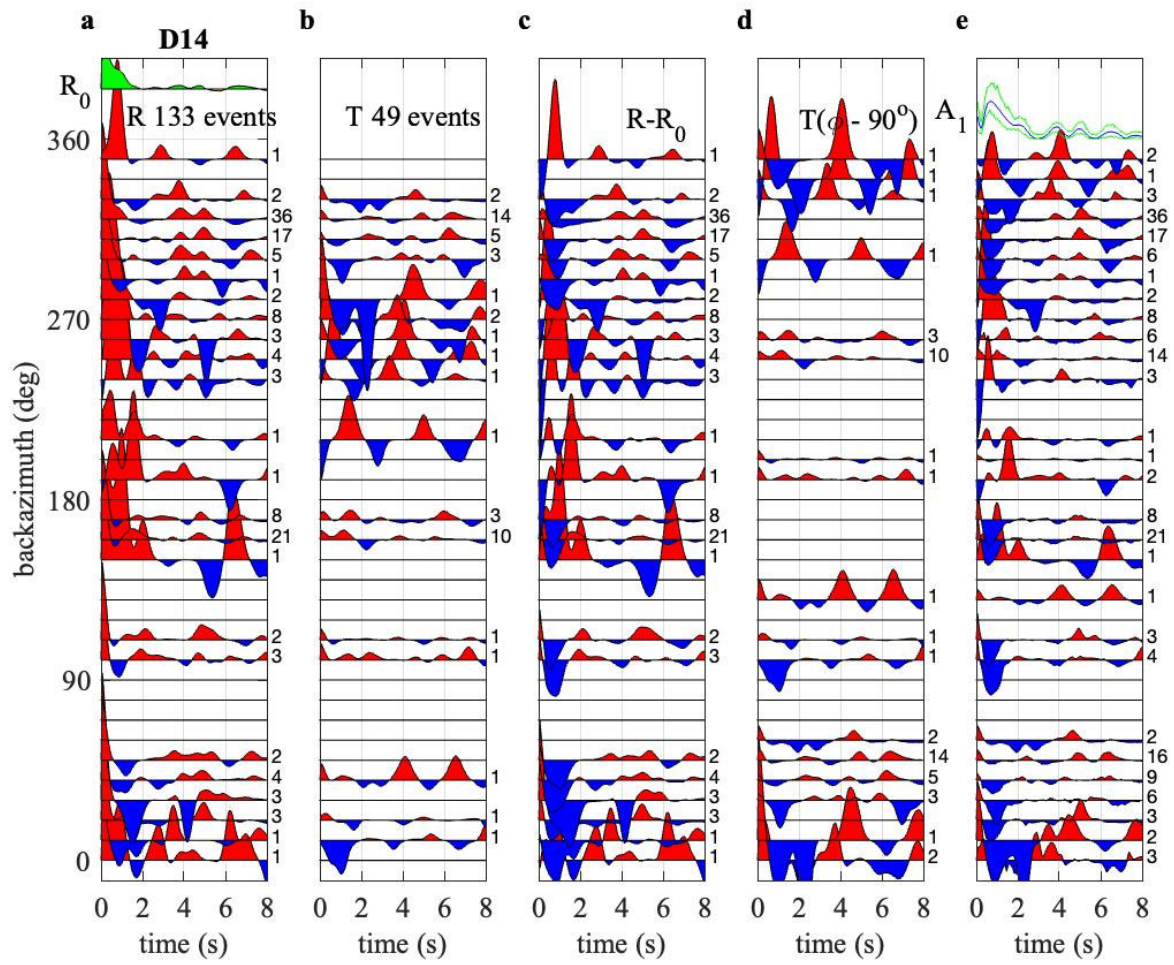


Figure S17. As in Fig. S5, but for SESAME station D14.

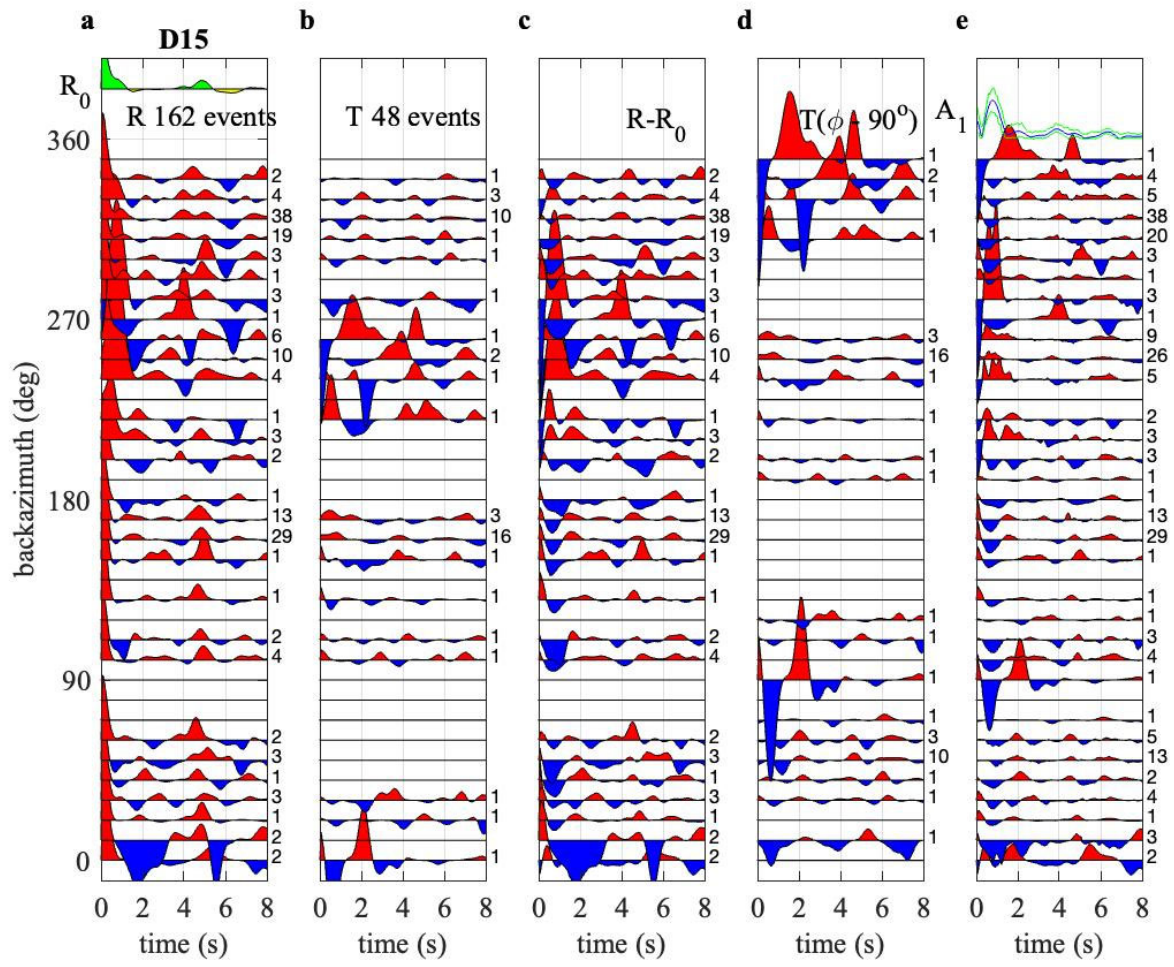


Figure S18. As in Fig. S5, but for SESAME station D15.

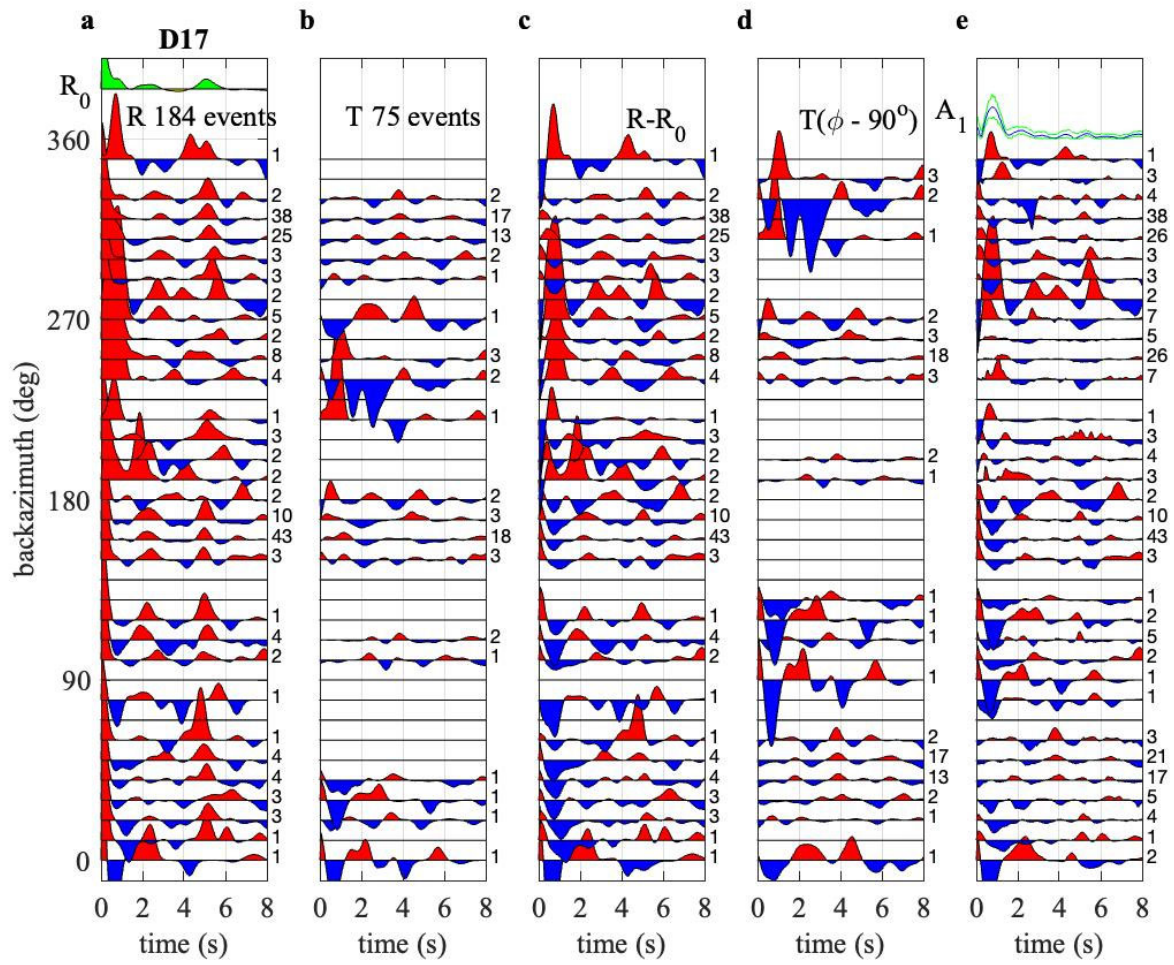


Figure S19. As in Fig. S5, but for SESAME station D17.

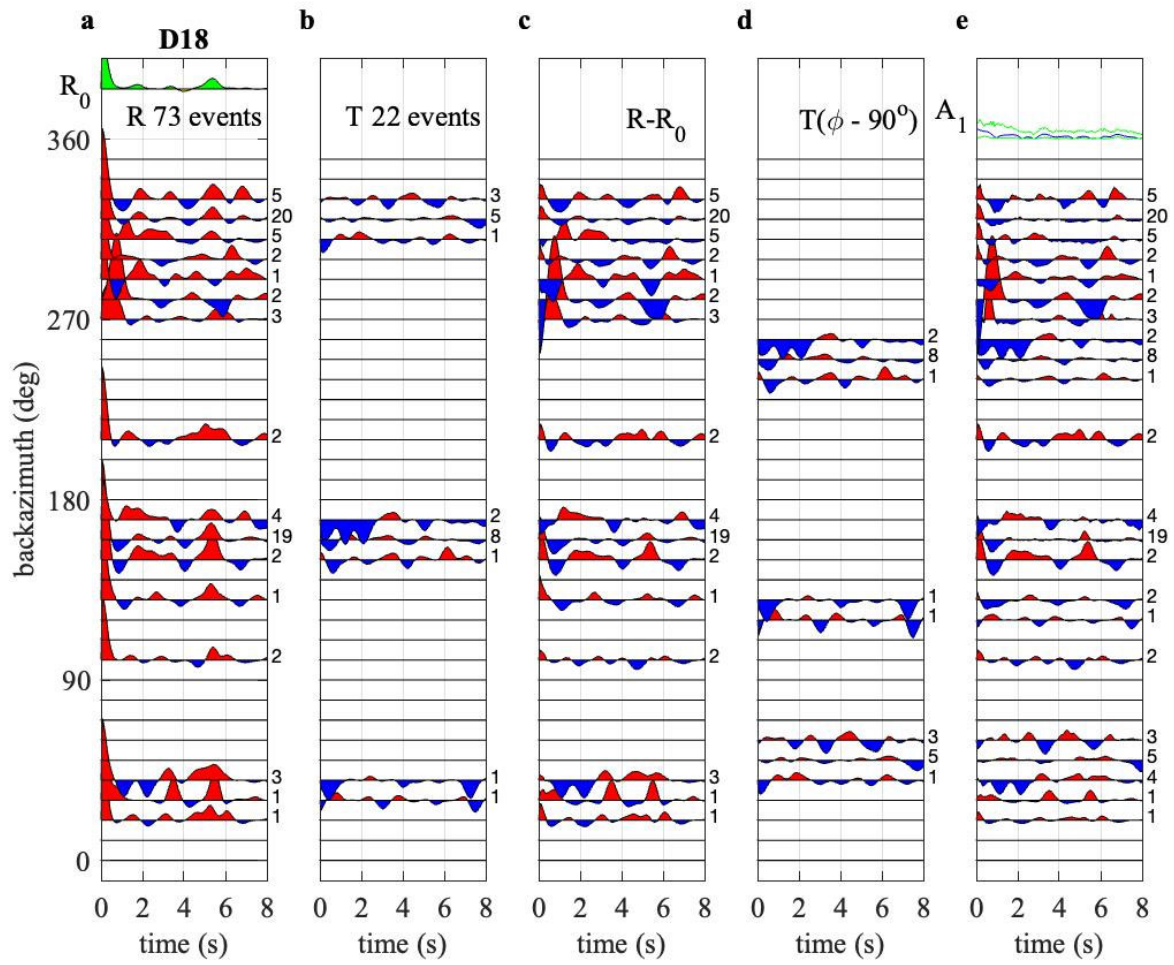


Figure S20. As in Fig. S5, but for SESAME station D18.

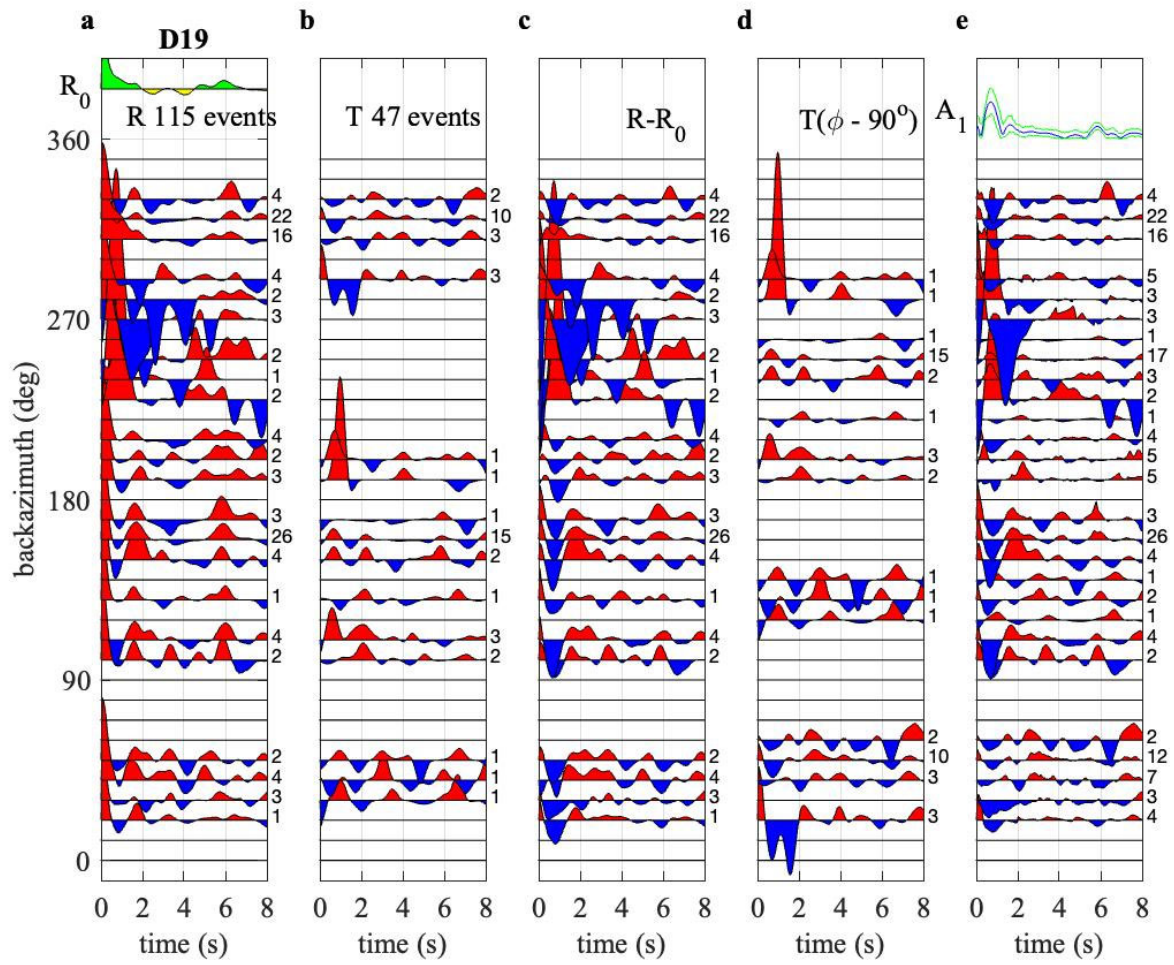


Figure S21. As in Fig. S5, but for SESAME station D19.

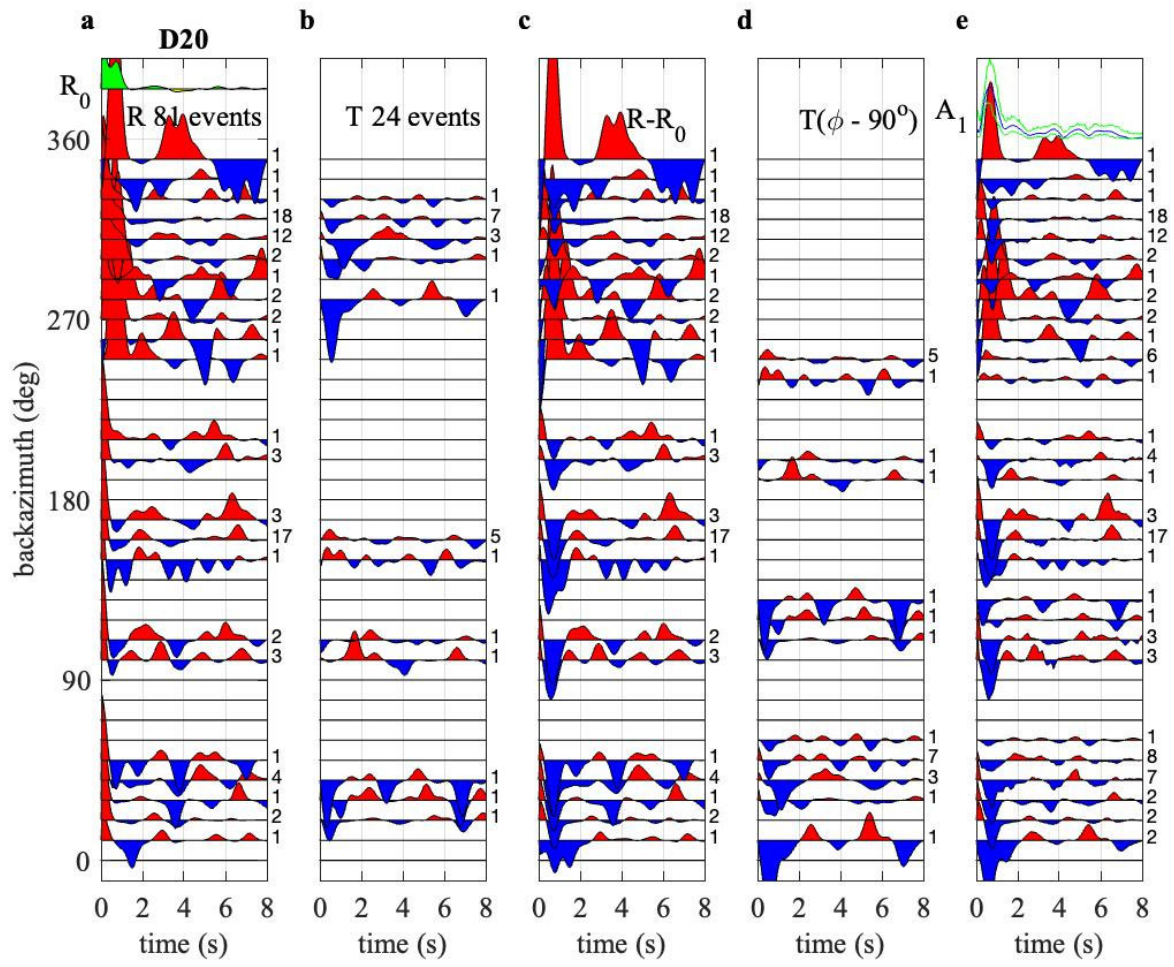


Figure S22. As in Fig. S5, but for SESAME station D20.

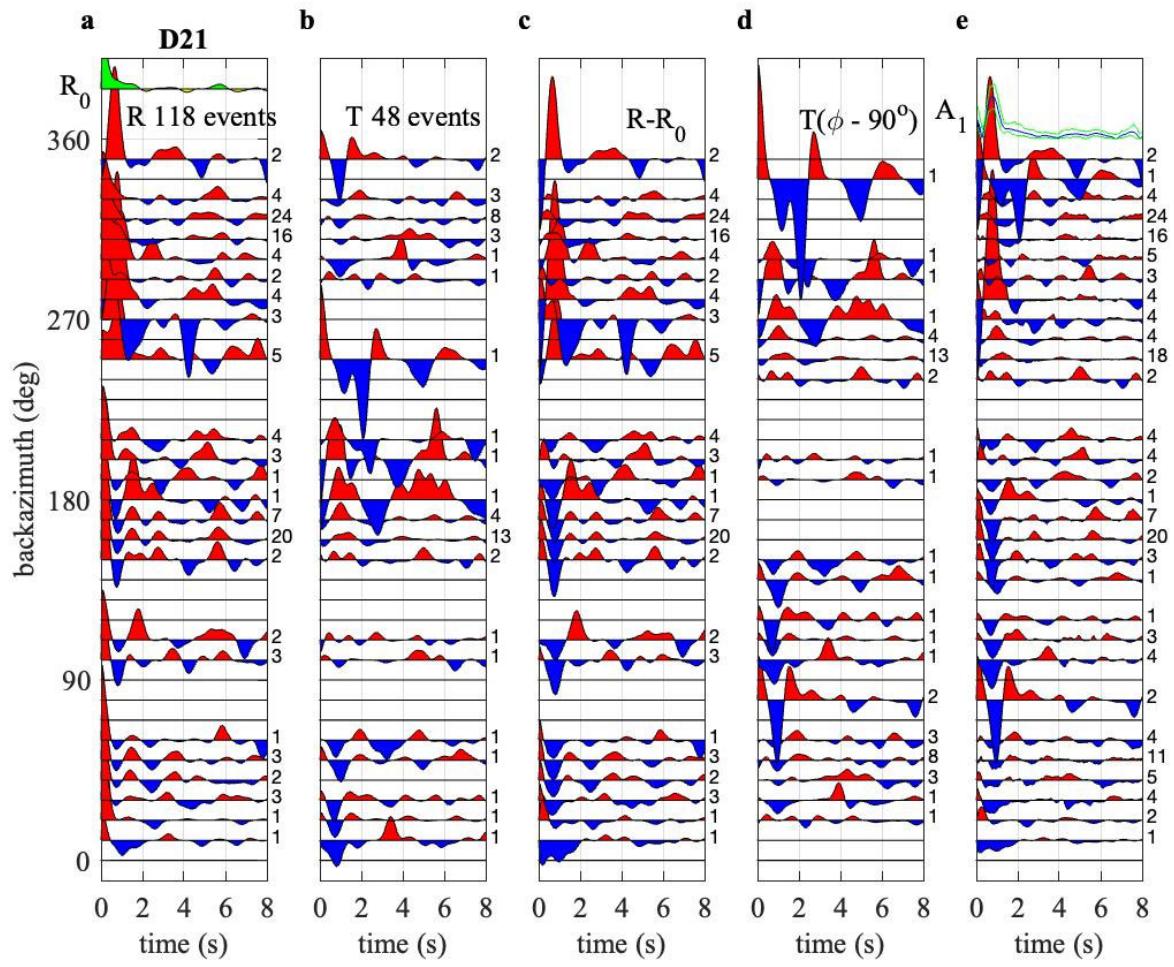


Figure S23. As in Fig. S5, but for SESAME station D21.

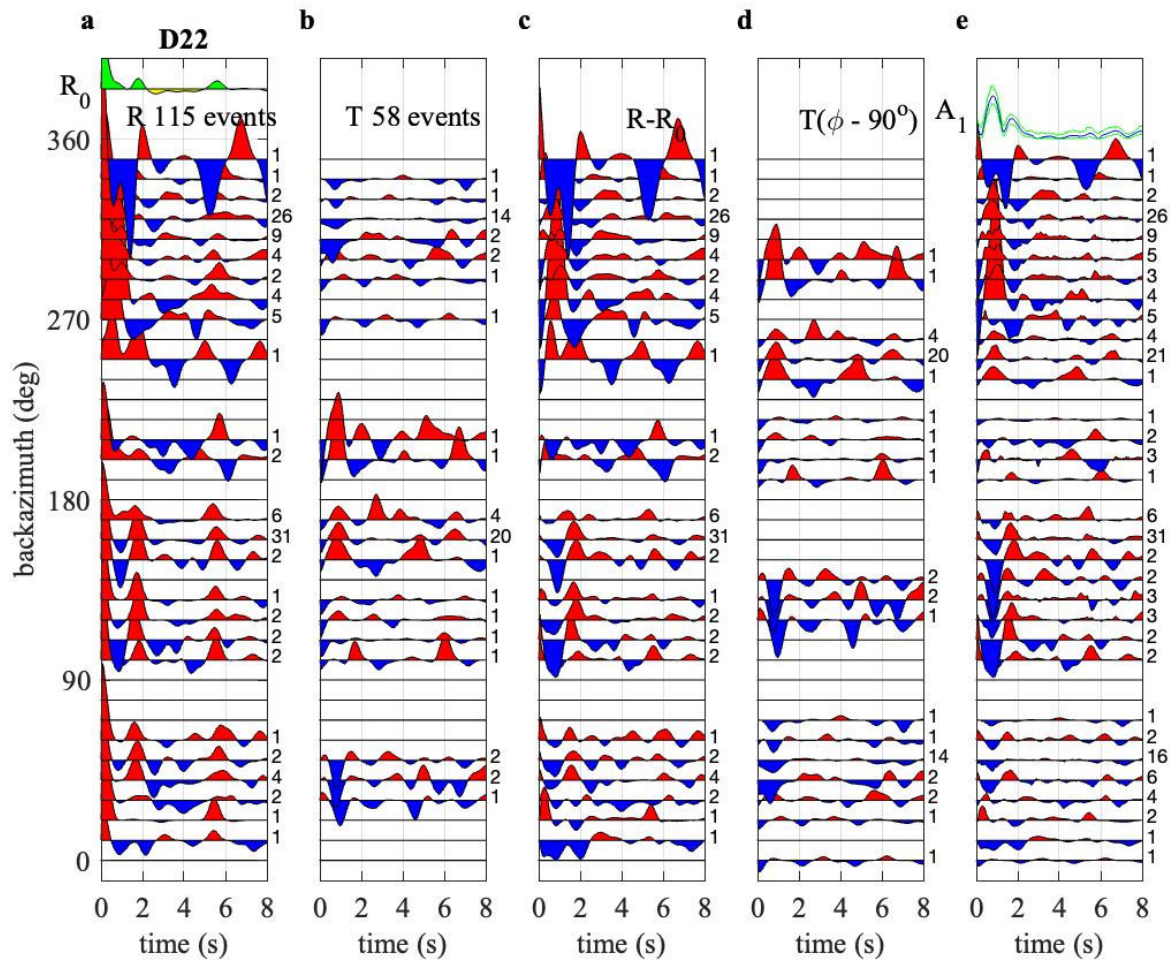


Figure S24. As in Fig. S5, but for SESAME station D22.

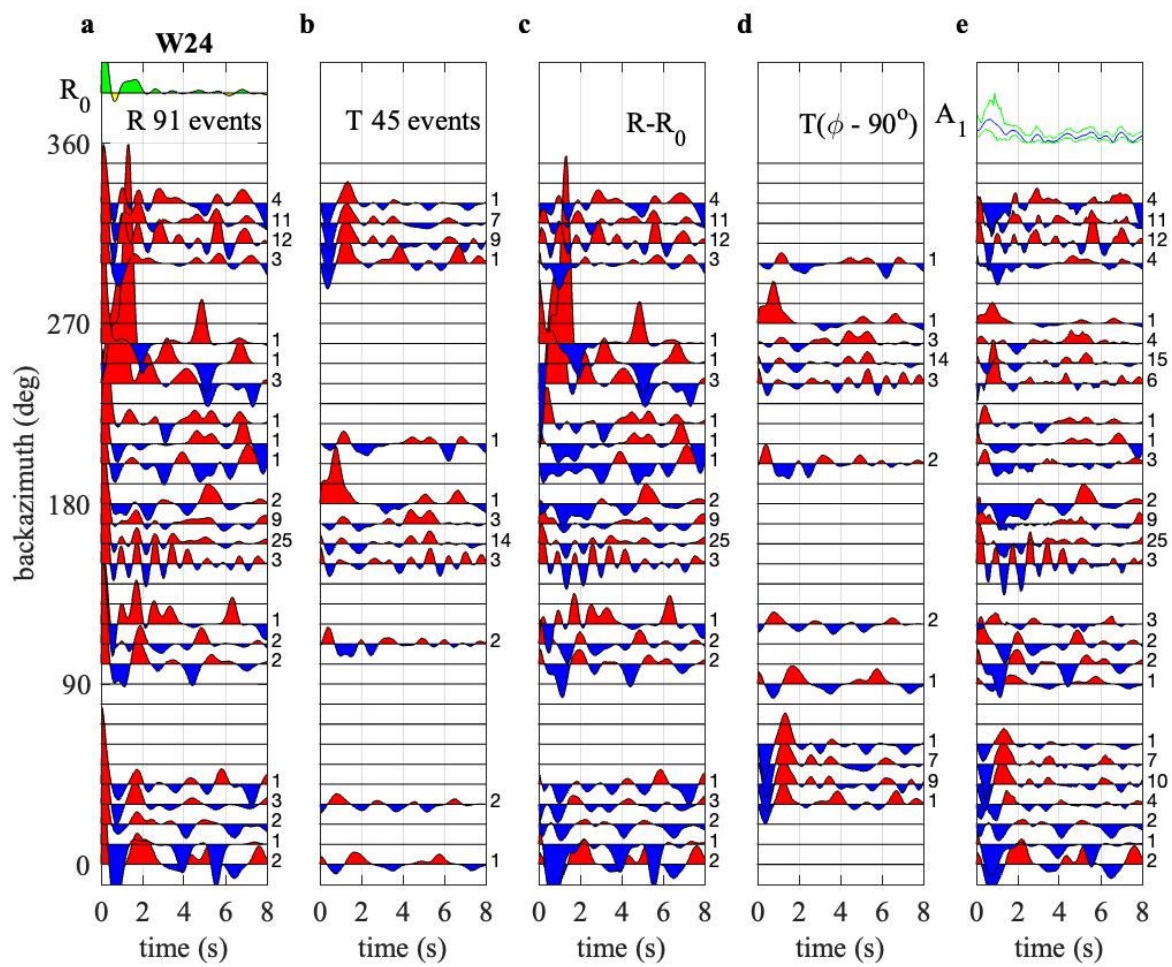


Figure S25. As in Fig. S5, but for SESAME station W24.

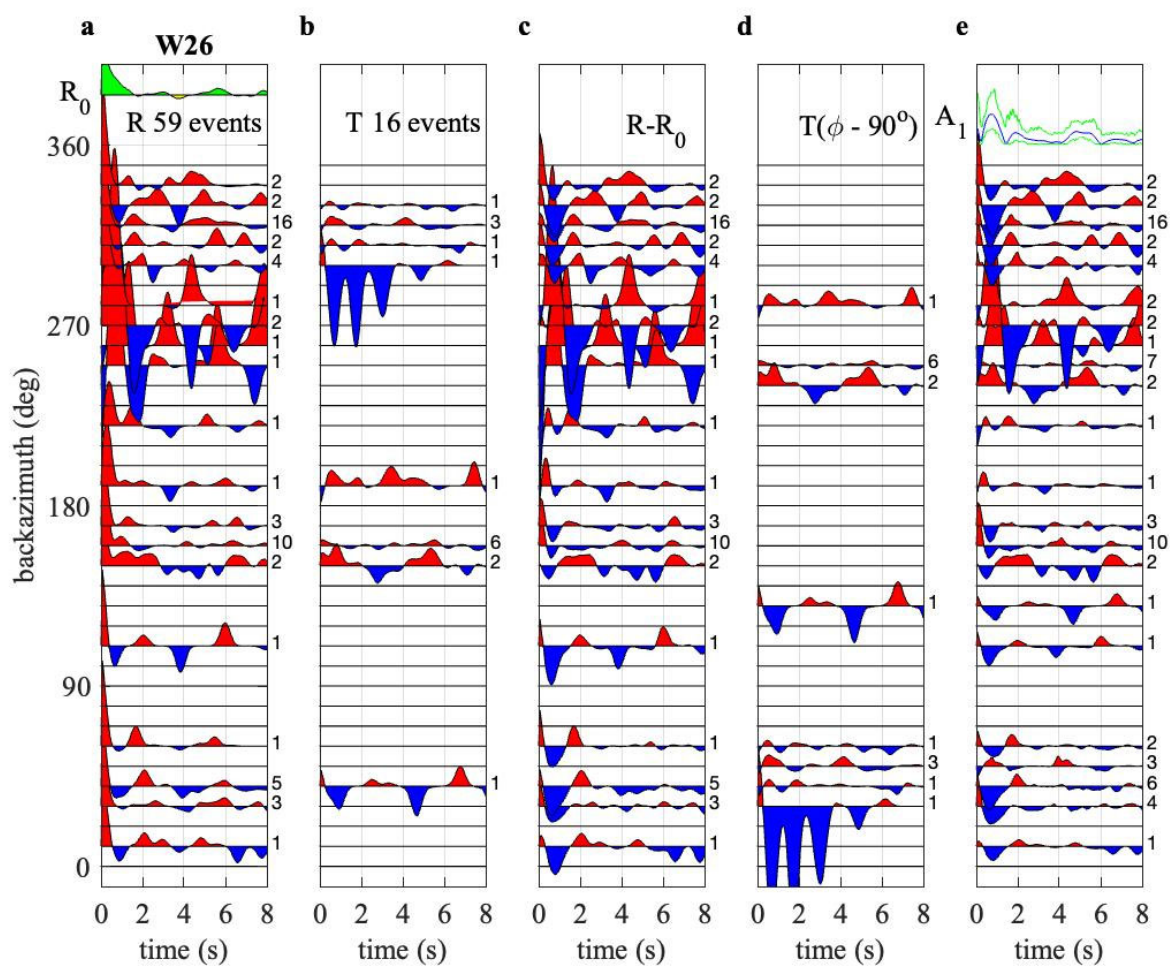


Figure S26. As in Fig. S5, but for SESAME station W26.

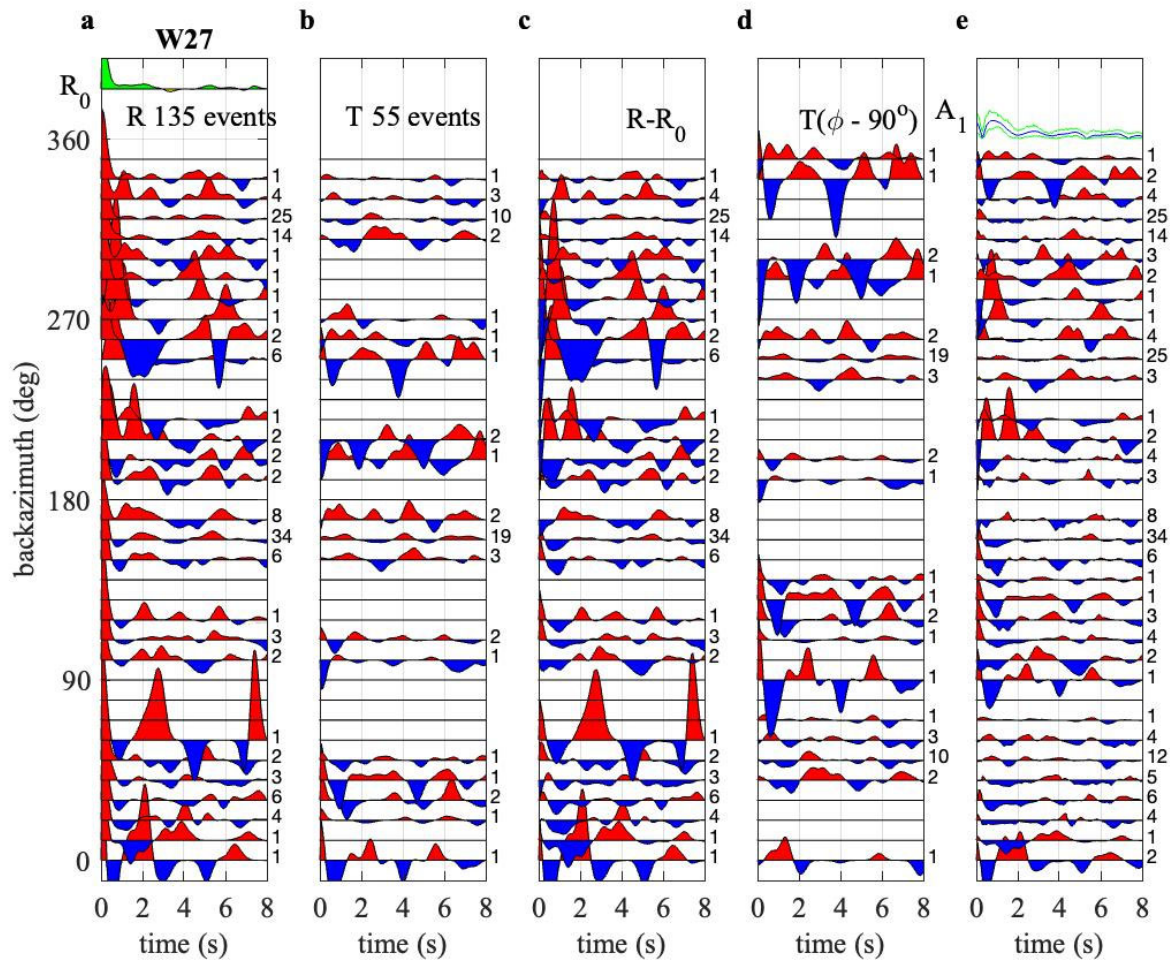


Figure S27. As in Fig. S5, but for SESAME station W27.

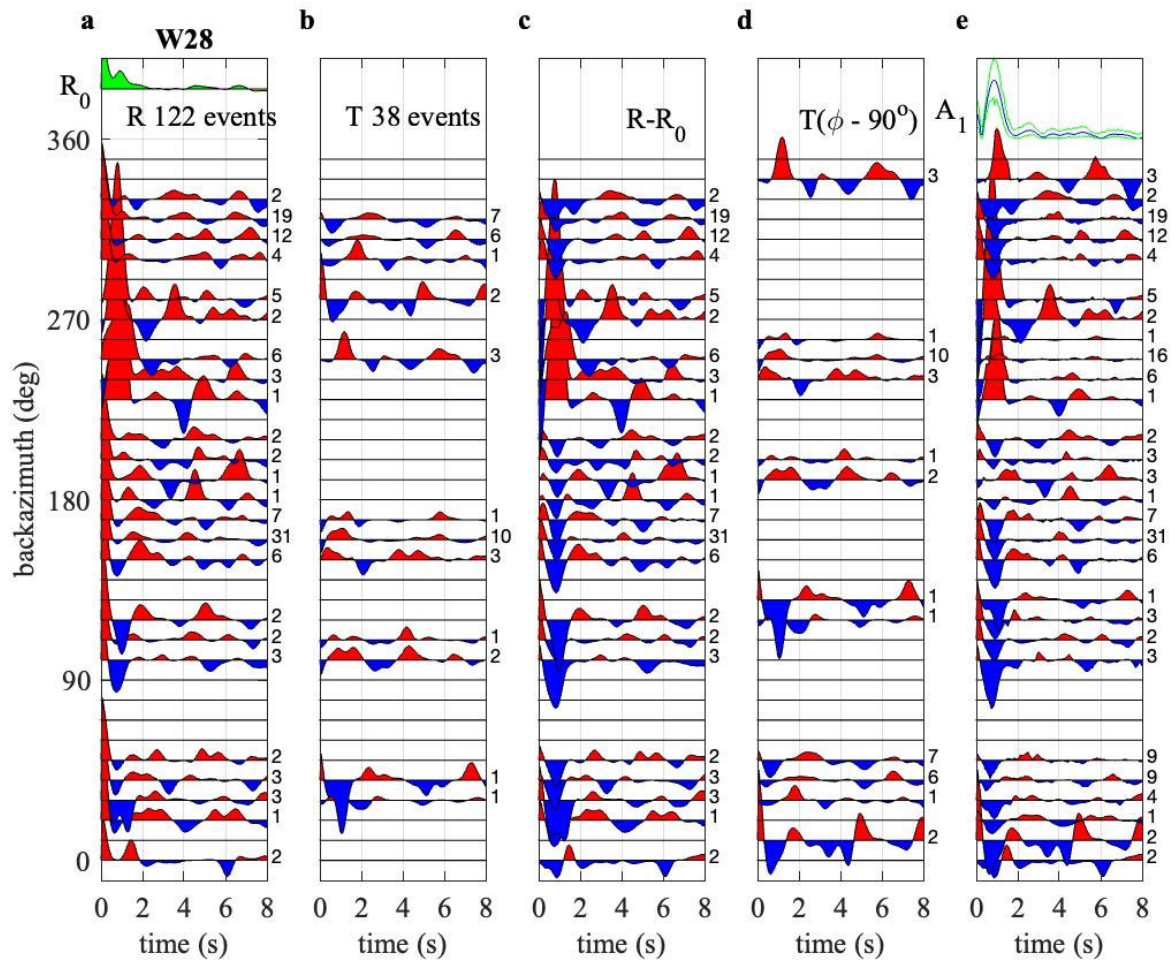


Figure S28. As in Fig. S5, but for SESAME station W28.

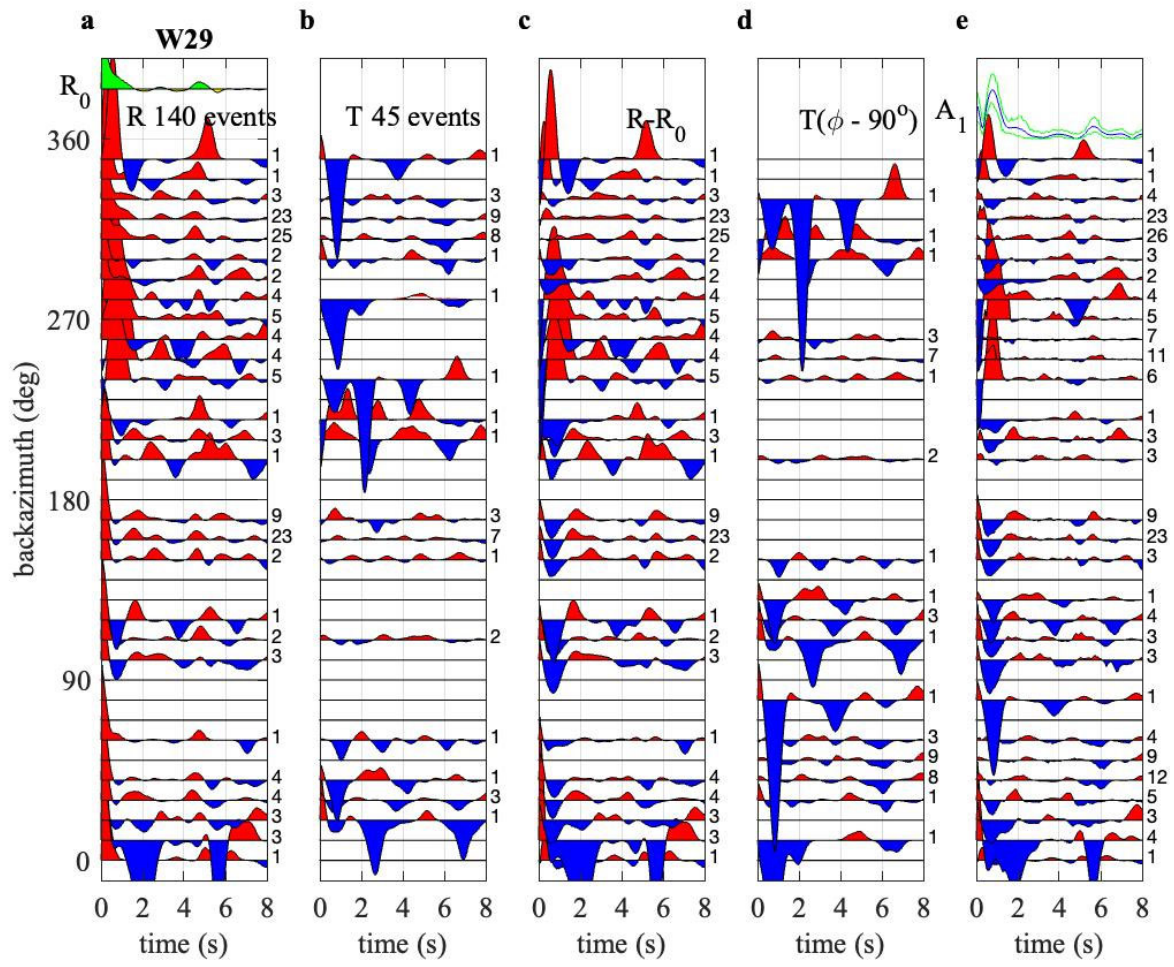


Figure S29. As in Fig. S5, but for SESAME station W29.

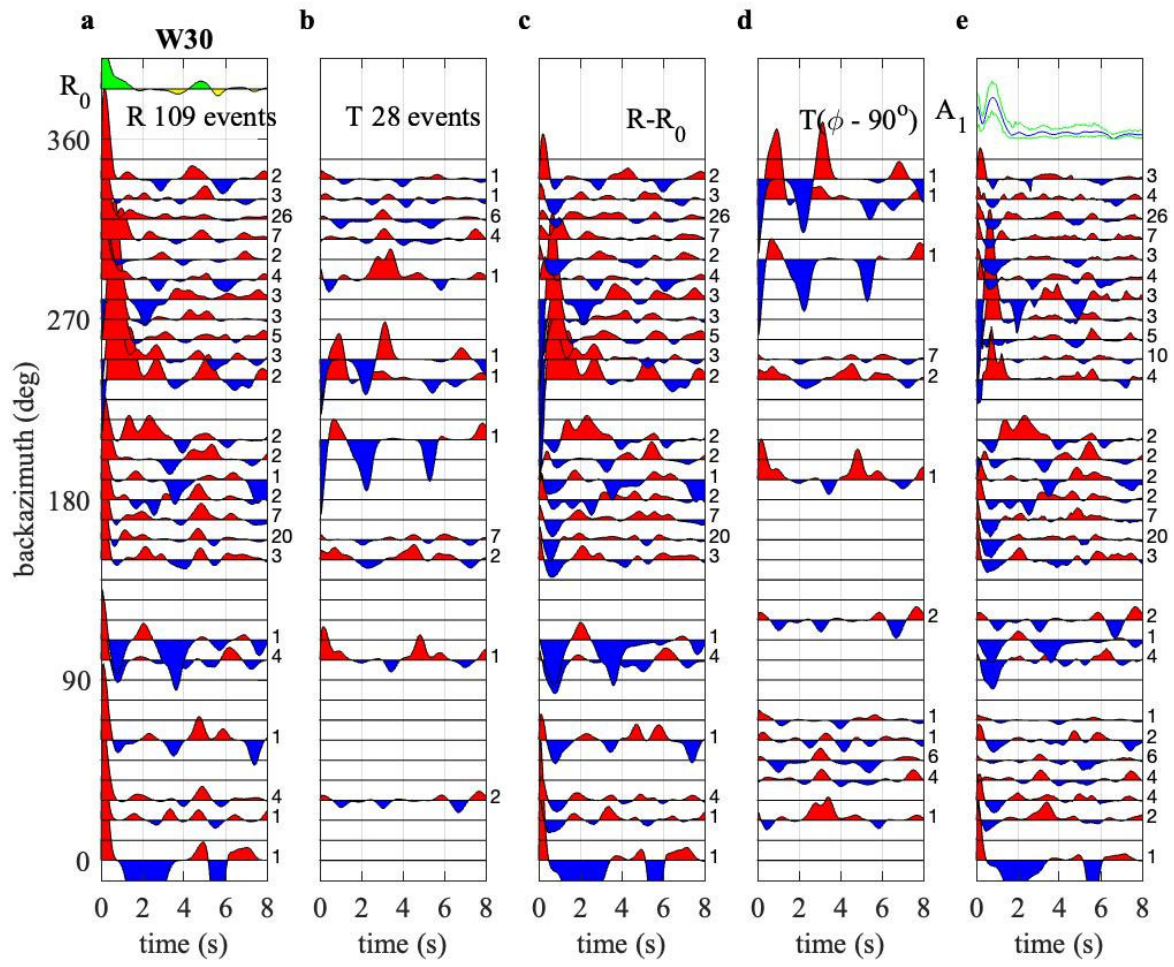


Figure S30. As in Fig. S5, but for SESAME station W30.

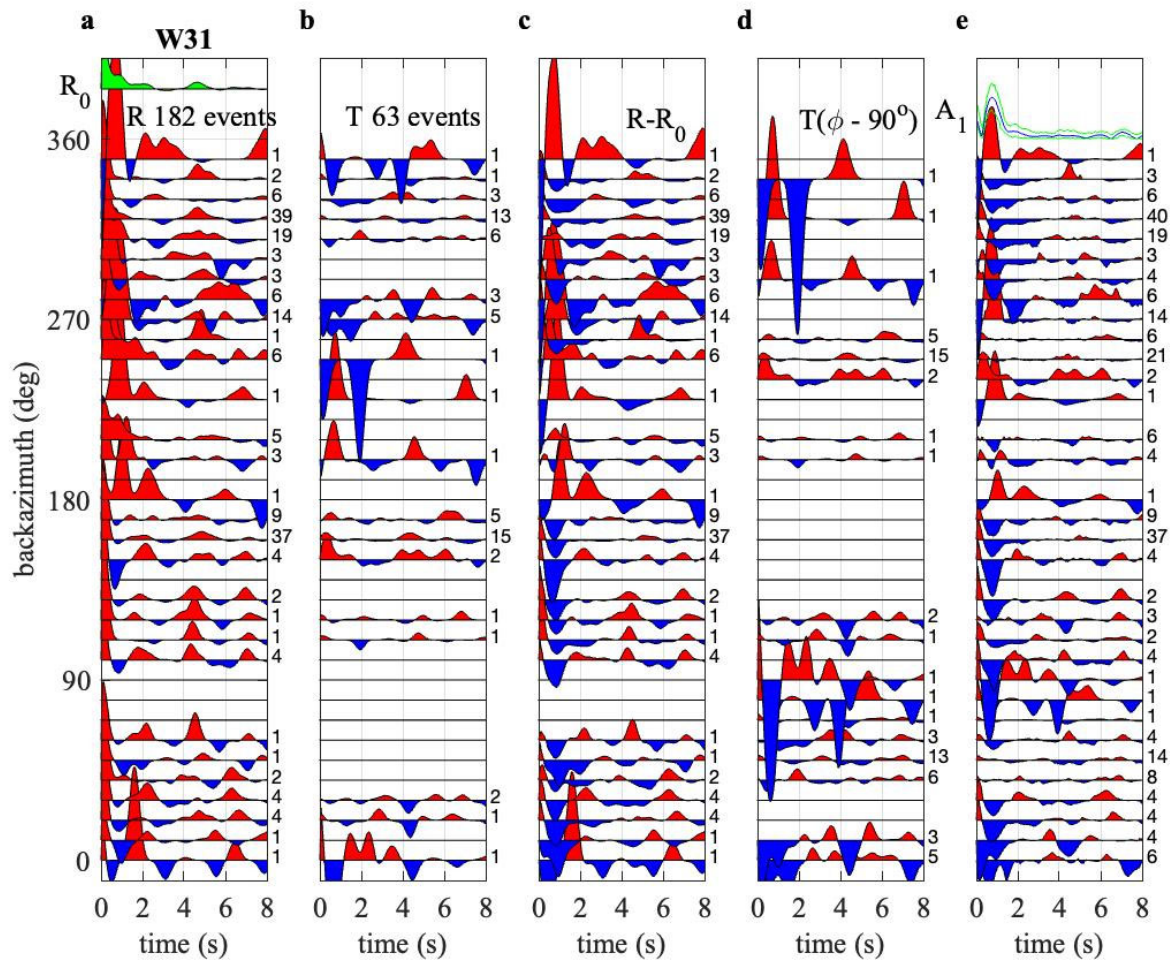


Figure S31. As in Fig. S5, but for SESAME station W31.

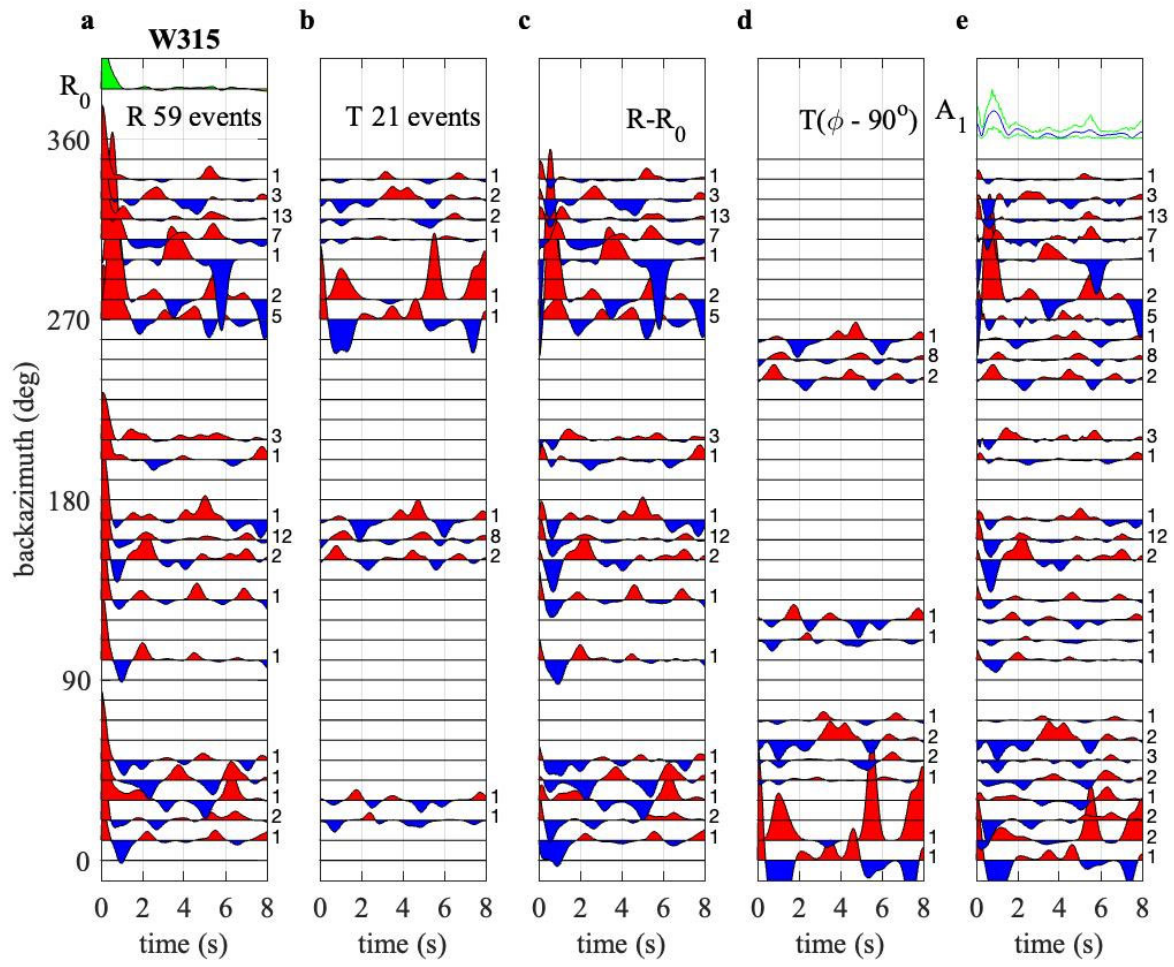


Figure S32. As in Fig. S5, but for SESAME station W315.

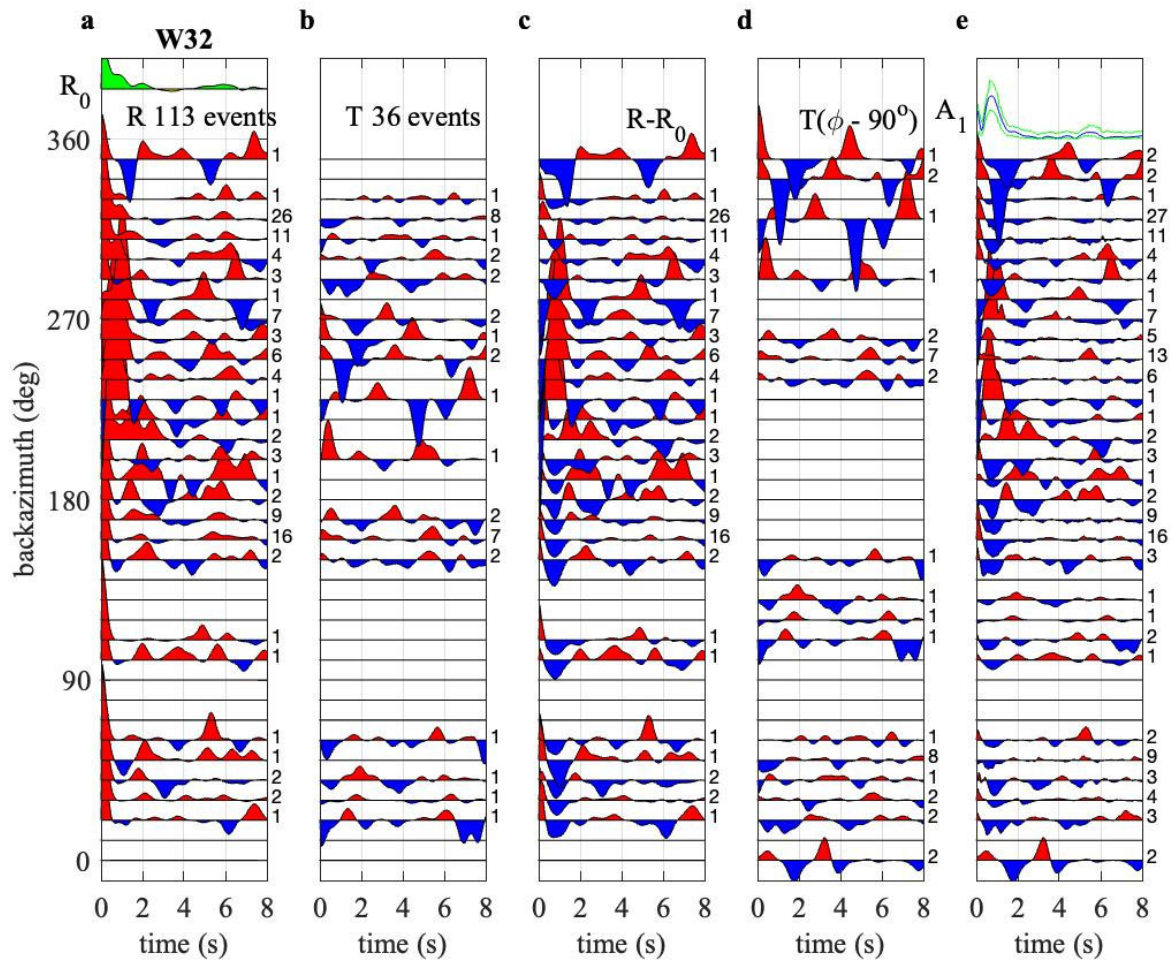


Figure S33. As in Fig. S5, but for SESAME station W32.

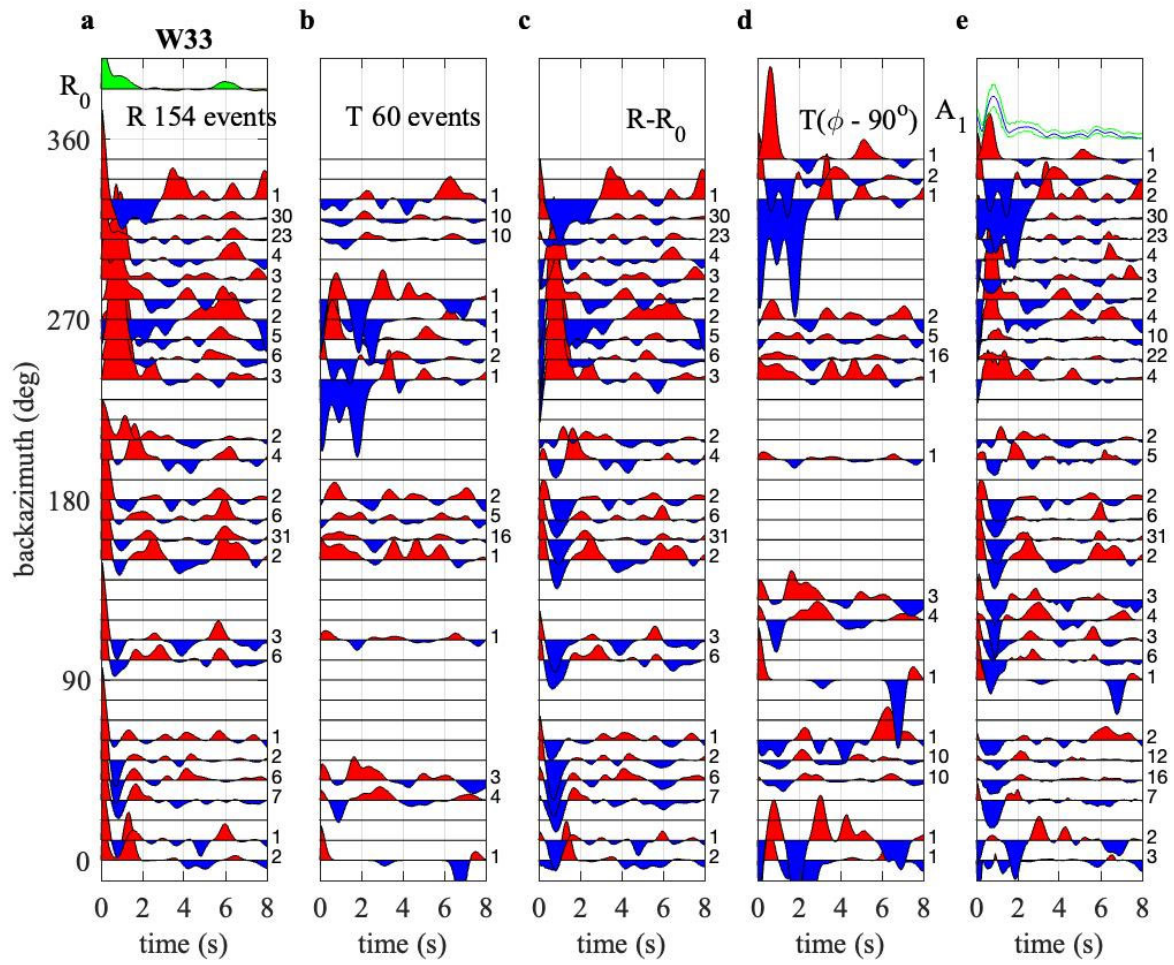


Figure S34. As in Fig. S5, but for SESAME station W33.

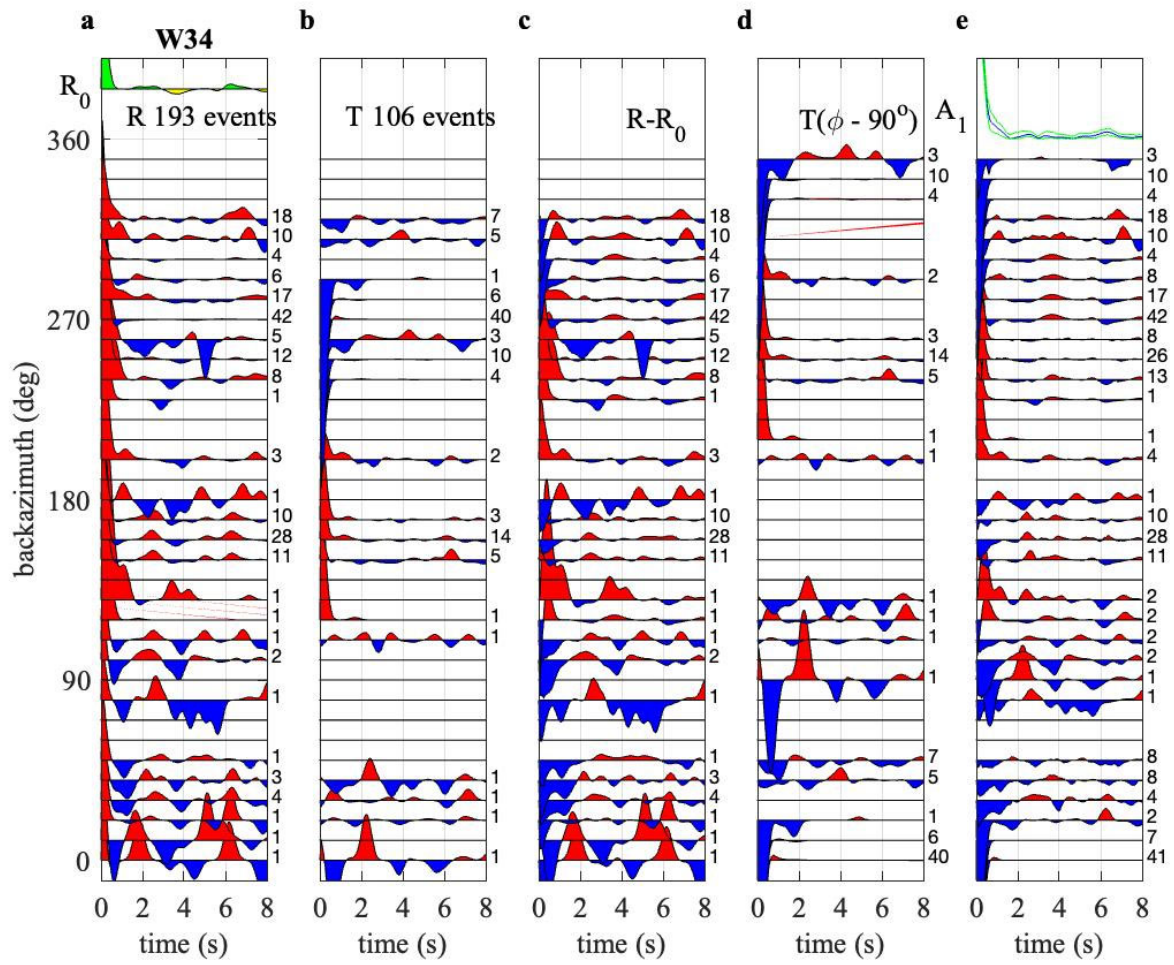


Figure S35. As in Fig. S5, but for SESAME station W34.

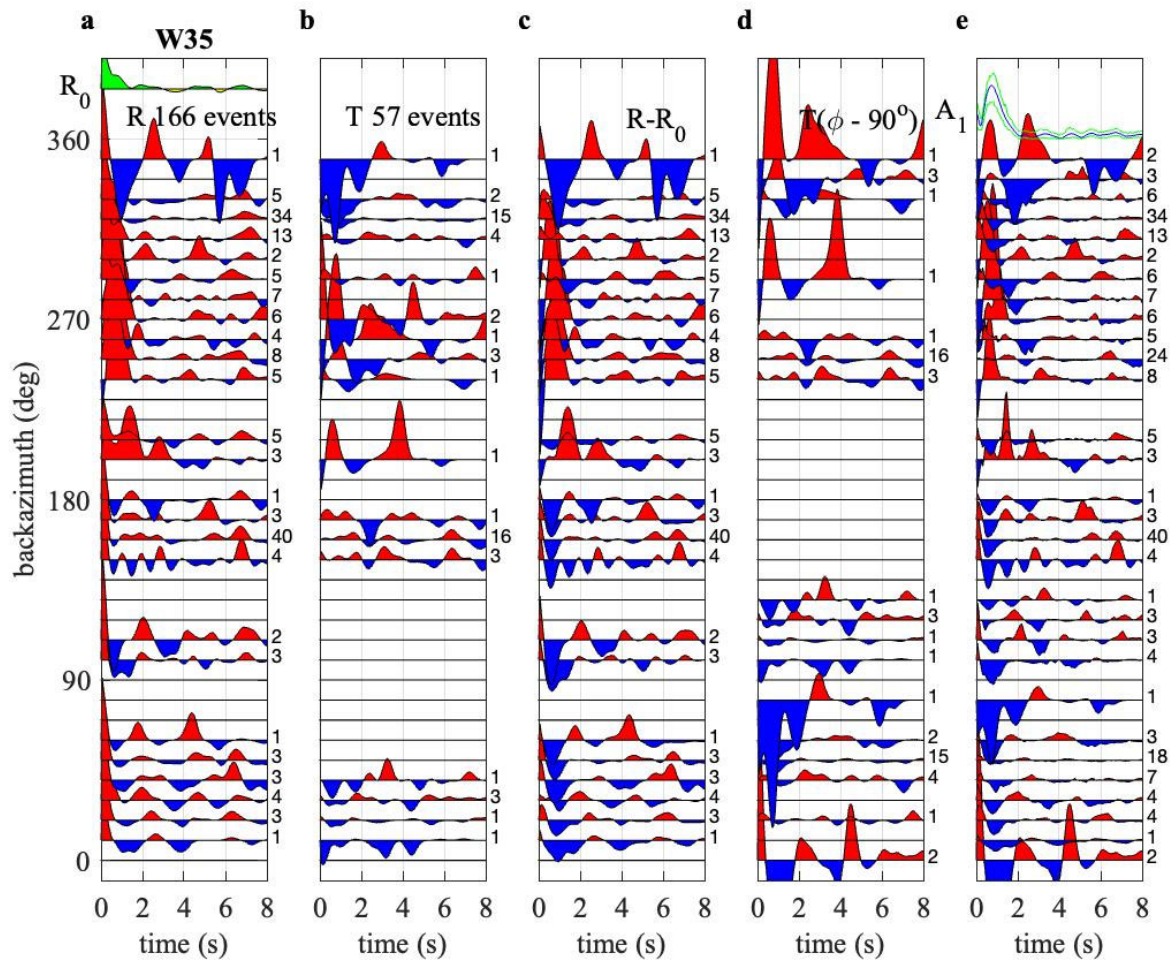


Figure S36. As in Fig. S5, but for SESAME station W35.

SUPPLEMENTAL REFERENCES

- Allmendinger, R.W., 2020, GMDE: Extracting quantitative information from geologic maps: *Geosphere*, v. 16(6), p. 1495-1507, <https://doi.org/10.1130/GES02253.1>
- Frothingham, M.G., Mahan, K.H., Schulte-Pelkum, V., Caine, J.S., and Vollmer, F.W., 2022, From crystals to crustal-scale seismic anisotropy: Bridging the gap between rocks and seismic studies with digital geologic map data in Colorado: *Tectonics*, v. 41, <https://doi.org/10.1029/2021TC006893>
- Hatcher, R.D., Jr., Bream, B.R., and Merschhat, A.J., 2007a, Tectonic map of the southern and central Appalachians: A tale of three orogens and a complete Wilson cycle, in Hatcher, R.D., Jr., et al., eds., 4-D Framework of Continental Crust: Geological Society of America Memoir 200, p. 1–38, [https://doi.org/10.1130/2007.1200\(29\)](https://doi.org/10.1130/2007.1200(29)).
- Nelson, A. E., Horton Jr., J. W., and Clarke, J. W., 1998, Geologic map of the Greenville 1 degree by 2 degrees Quadrangle, Georgia, South Carolina, and North Carolina: U.S. Geological Survey IMAP 2175, scale 1:250,000, <https://doi.org/10.3133/i2175>
- Schulte-Pelkum, V., and Mahan, K.H., 2014, A method for mapping crustal deformation and anisotropy with receiver functions and first results from USArray: *Earth and Planetary Science Letters*, v. 402, p. 221-233, <https://doi.org/10.1016/j.epsl.2014.01.050>
- Schulte-Pelkum, V., Ross, Z.E., Mueller, K., and Ben-Zion, Y., 2020a, Tectonic Inheritance With Dipping Faults and Deformation Fabric in the Brittle and Ductile Southern California Crust: *Journal of Geophysical Research: Solid Earth*, v. 125(8), p. 1-15, <https://doi.org/10.1029/2020JB019525>
- Vollmer, F.W., 2015, Orient 3: A new integrated software program for orientation data analysis, kinematic analysis, spherical projections, and Schmidt plots: *Geological Society of America Abstracts With Programs*, v. 47(7), p. 49.

Any use of trade, firm, or product names is for descriptive purposes only and does not imply endorsement by the U.S. Government.